AN INVESTIGATION OF THE USE OF THE HOT-WIRE ANEMOMETER IN NON-ISOTHERMAL AIR FLOW

A Thesis

Submitted to the Faculty

of

Purdue University

by

Edwin George Wiggins

In Partial Fulfillment of the

Requirements for the Degree

of

Master of Science

in

Nuclear Engineering

January 1969

ACKNOWLEDGEMENTS

The author is indebted to Professor Alexander Sesonske for his advice and guidance throughout the course of this investigation.

Financial support from the National Science Foundation and the United States Navy, through the Junior Line Officer Advanced Scientific Education Program, is gratefully acknowledged.

TABLE OF CONTENTS

TABLE OF CONTENTS
(Continued)

LIST OF TABLES

LIST OF FIGURES

LIST OF FIGURES
(Continued)

NOMENCLATURE

Symbol	Definition	Dimensions
A	Empirical constant	
a	Empirical constant	volts/^{o}F
B	Empirical constant	
C	Defined by Equation 17	$(\frac{volts}{ohms})^2 (\frac{ft}{sec})^{\frac{1}{2}}$
C_p	Specific heat of air	BTU/lb ^{o}F
D	Diameter of hot-wire	inch
E	Instantaneous hot-wire/thermocouple voltage	volts
$\bar{E}$	D.C. component of hot-wire/thermocouple voltage	volts
$\bar{E}_o$	Thermocouple reference voltage	volts
e'	Fluctuating component of hot wire/thermocouple voltage	millivolts
h	Convective heat transfer coefficient	BTU/hr·ft^2·^{o}F
k	Thermal conductivity of air	BTU/hr·ft·^{o}F
$\bar{k}$	Time average thermal conductivity of air	BTU/hr·ft·^{o}F
k'	Fluctuating component of thermal conductivity of air	BTU/hr·ft·^{o}F
ℓ	Length of hot wire	inch
m	Empirical constant	
Nu	Nusselt number	
ΔP	Pressure difference between points upstream and downstream of orifice plate	inches of manometer fluid
Pr	Prandtl Number of air	
q"	Heat flux from surface of hot-wire	BTU/hr·ft^2

R	Pipe radius	inch
r	Distance from pipe centerline	inch
R_a	Hot-wire resistance at local air temperature	ohm
$\bar{R}_a$	Hot-wire resistance at time average local air temperature	ohm
R_o	Hot-wire reference resistance	ohm
R_w	Hot-wire resistance at operating temperature	ohm
r'_a	Fluctuating hot-wire resistance corresponding to fluctuating component of local air temperature	ohm
Re	Reynolds Number	
S_u	Hot-wire sensitivity to velocity fluctuations	millivolts/ft/sec
S_T	Hot-wire sensitivity to temperature fluctuations	millivolts/^oF
T, T_a	Instantaneous local air temperature	^oF
$T, \bar{T}_a$	Time average local air temperature	^oF
$T_{℄}$	Time average temperature at pipe centerline	^oF
T_o	Wall temperature	^oF
T_w	Wire temperature	^oF
t'	Fluctuating component of local air temperature	^oF
u	Instantaneous local flow velocity	ft/sec
$\bar{u}$	Time average local flow velocity	ft/sec
u'	Fluctuating component of local flow velocity	ft/sec
α	Hot-wire resistivity coefficient	$^oF^{-1}$
ρ	Instantaneous air density	lb/ft^3
$\bar{\rho}$	Time average air density	lb/ft^3
ρ'	Fluctuating component of air density	lb/ft^3

ABSTRACT

Wiggins, Edwin George, M.S. in Nuclear Engineering, Purdue University, January 1969. An Investigation of the Use of the Hot-Wire Anemometer in Non-Isothermal Air Flow. Major Professor: Alexander Sesonske.

Procedures were developed for the calibration of the hot-wire anemometer in a non-isothermal flow. Various methods of using the results of calibration to compute turbulent fluctuations of velocity and temperature were considered, and the Arya and Plate modification of the Kovasznay Fluctuation Diagram method was found to give the most accurate results. The method requires independent measurement of the temperature fluctuations which was obtained with a rapid response thermocouple.

The calculated values of velocity turbulence intensity show deviations of 36 percent from the results of Laufer; however, this deviation is to be expected in view of the estimated experimental error. These errors were probably caused by contamination of the wire during the lengthy calibration process.

All measurements were made in air flowing in a 1.0625 inch diameter pipe at Reynolds Numbers between 30,000 and 50,000. A heat input of 430 watts over the last 58 inches before the probe was used to generate temperature differences between wall and centerline of 48 to 63°F at the probe location.

The procedures developed and the experimental problems identified are the contribution of this investigation to a comprehensive research program of non-isothermal hot-wire measurements in fluids of a wide range of Prandtl Numbers.

INTRODUCTION

The hot-wire anemometer has been used extensively for the measurement of velocity fluctuations in isothermal flow of gases. The principles and procedures involved are discussed by Kovasznay[1,2] and by Kronauer[3].

Corrsin[4] has shown that in addition, the hot-wire anemometer has the potential to measure simultaneous velocity and temperature fluctuations in non-isothermal flow. Experimental work of this nature has been done by Corrsin and Uberoi[5], Gibson Chen and Lin[6], Deissler[7], Kunstman[8], and Arya and Plate[9]. The present work was concerned with the development of experimental procedures and the identification of problems associated with making of such measurements in a non-isothermal air flow.

In isothermal flow the only flow variable affecting the anemometer output is the velocity. Thus the anemometer voltage fluctuation is directly proportional to the velocity fluctuation and the anemometer steady voltage is directly proportional to the mean velocity.

In non-isothermal flow, however, both the velocity and ambient temperature fluctuations affect the anemometer output. Considerable difficulty has been encountered by previous workers in separating the two effects. Errors up to 750 percent[8] have been reported in non-isothermal measurements, while in isothermal measurements 10 percent error or less is expected.

The non-isothermal flow measurements of the present work were preceeded by velocity fluctuation measurements in isothermal flow with a

hot-wire paralleling the work of Laufer[10] and Sandborn[11] and temperature fluctuation measurements in non-isothermal flow with a rapid response thermocouple. Thus the velocity and temperature fluctuation intensities measured with the hot-wire in non-isothermal flow could be compared with results of more direct measurements.

THEORETICAL BACKGROUND

The constant temperature hot-wire anemometer consists of a fine tungsten or platinum wire maintained by a feedback system at some constant temperature above that of the fluid in which it is inserted. The convective heat loss from the wire is balanced by joulean heating of the wire by the current supplied by the feedback system.

King[12] solved the convection problem by assuming potential flow around the wire and obtained the following relationship:

$$Nu = (A + BRe^{\frac{1}{2}})\ \left(1 + \tfrac{1}{2}\,\frac{T_w - T_a}{T_a}\right)^m ,$$

where $Re = \dfrac{Du\rho}{\mu}$.

Although it is recognized that King's assumptions are unacceptable, the functional form of his relationship has proved to be a satisfactory representation of experimental data. Thus it is seen that the joulean heating current (or voltage) required to maintain the wire at a constant temperature is a function of the instantaneous velocity of the flow and the difference in temperature between wire and fluid.

In isothermal flow, the temperature difference is constant and the system can be used to measure the mean and fluctuating components of the instantaneous velocity. In non-isothermal flow the fluid temperature has a fluctuating component that affects the heat transfer in addition to the effect of the fluctuating component of the velocity. Thus in

principle, the system can be used to measure velocity and temperature fluctuations, since it is sensitive to both fluctuations.

Hot-Wire in Isothermal Flow

The following parallels Corrsin's[4] treatment for a constant current hot-wire anemometer. For heat transfer to flow over a cylinder:

$$Nu = (A + B\ Re^{1/2})\left[1 + \frac{1}{2}\frac{T_w - T_a}{T_a}\right]^m . \tag{1}$$

In the range of interest,

$$\frac{1}{2}\frac{T_w - T_a}{T_a} << 1. \tag{2}$$

Thus Equation 1 may be simplified to

$$Nu = A + B\ Re^{1/2}. \tag{3}$$

By definition,

$$Nu = \frac{hD}{k} = \frac{q''D}{k(T_w - T_a)} . \tag{4}$$

For electrical resistance heating,

$$q'' = \frac{E^2}{R_w \pi D \ell} . \tag{5}$$

Substitution of Equations 4 and 5 into 3 yields

$$\frac{E^2}{R_w(T_w - T_a)} = (\pi k \ell A) + (\pi k \ell B)\ Re^{1/2} \tag{6}$$

By definition,

$$Re = \frac{\rho u D}{\mu} . \tag{7}$$

Thus,

$$\frac{E^2}{R_w(T_w - T_a)} = (\pi k \ell A) + (\pi k \ell B \left[\frac{\rho D}{\mu} \right]^{1/2}) u^{1/2}. \tag{8}$$

The quantities in parentheses on the right side of Equation 8 are constants. For constant temperature operation of the hot-wire in an isothermal flow the following mean and deviation quantities are used:

$$u = \overline{u} + u' \quad \text{and} \quad E = \overline{E} + e'. \tag{9}$$

Substitution of Equations 9 into Equation 8 yields, after small terms have been discarded,

$$\frac{\overline{E}^2 + 2\overline{E}e'}{R_w(T_w - T_a)} = (\pi k \ell A) + (\pi k \ell B \left[\frac{\rho D}{\mu} \right]^{1/2}) \overline{u}^{1/2} (1 + \frac{u'}{\overline{u}})^{1/2} \tag{10}$$

By definition,

$$T_w - T_a = \frac{1}{\alpha R_o} (R_w - R_a). \tag{11}$$

According to the binomial theorem

$$(1 + \frac{u'}{u})^{1/2} = 1 + \frac{1}{2} \frac{u'}{\overline{u}} + \cdots . \tag{12}$$

Since $\frac{u'}{u} << 1$, it is assumed that higher order terms may be neglected in Equation 12. Thus Equation 10 becomes

$$\frac{\overline{E}^2}{R_w(R_w - R_a)} + \frac{2\overline{E}e'}{R_w(R_w - R_a)} = (\frac{\pi k \ell}{\alpha R_o} A) + (\frac{\pi k \ell}{\alpha R_o} B \left[\frac{\rho D}{\mu}\right]^{1/2}) (\overline{u}^{1/2} + \frac{u'}{2\overline{u}^{1/2}}). \tag{13}$$

Time averaging of Equation 13 yields

$$\frac{\overline{E}^2}{R_w(R_w - R_a)} = (\frac{\pi k \ell}{\alpha R_o} A) + (\frac{\pi k \ell}{\alpha R_o} B \left[\frac{\rho D}{\mu} \right]^{1/2}) \overline{u}^{1/2}. \tag{14}$$

Subtraction of Equation 14 from 13 gives

$$\frac{2\bar{E}e'}{R_w(R_w - R_a)} = \left(\frac{\pi k \ell}{\alpha R_o} B\left[\frac{\rho D}{\mu} \right]^{1/2} \right) \frac{u'}{2\bar{u}^{1/2}} , \tag{15}$$

or

$$\frac{4\bar{E}e'}{R_w(R_w - R_a)\, C\bar{u}^{1/2}} = \frac{u'}{\bar{u}} . \tag{16}$$

Note that

$$C = \frac{\pi k \ell}{\alpha R_o} B \left[\frac{\rho D}{\mu} \right]^{1/2} , \tag{17}$$

and that this same quantity appears as the coefficient of $\bar{u}^{\frac{1}{2}}$ in Equation 14. Squaring, time averaging, and taking the square root of Equation 16 yields

$$\frac{4\bar{E}\sqrt{\overline{e'^2}}}{R_w(R_w - R_a)\, C\bar{u}^{1/2}} = \frac{\sqrt{\overline{u'^2}}}{\bar{u}} \tag{18}$$

Rapid Response Thermocouple in Non-Isothermal Flow

The behavior of a thermocouple over a fairly large range of temperature may be expressed as

$$E = E_o + aT . \tag{19}$$

The following fluctuating quantities are introduced:

$$E = \bar{E} + e' \quad \text{and} \quad T = \bar{T} + t' . \tag{20}$$

Substitution of Equations 20 into 19 yields

$$\bar{E} + e' = E_o + a(\bar{T} + t'). \tag{21}$$

Time averaging of Equation 21 yields

$$\overline{E} = E_o + a\overline{T} \quad . \tag{22}$$

Subtracting Equation 22 from 21 yields

$$e' = at' \tag{23}$$

Squaring, time averaging, and taking the square root of Equation 23 gives

$$\sqrt{\overline{e'^2}} = a\sqrt{\overline{t'^2}} \quad . \tag{24}$$

Hot-Wire in Non-Isothermal Flow

The following parallels Corrsin's[4] treatment for a constant current hot wire anemometer.

Equation 8 is still valid, however, ρ and k are no longer constants. Substitution of Equation 11 into 8 yields

$$\frac{E^2}{R_w(R_w-R_a)} = \left(\frac{\pi \ell}{\alpha R_o} A\right)k + \left(\frac{\pi \ell D^{1/2}}{\alpha R_o} \cdot \left[\frac{k}{C_p \mu}\right]^{1/2} B\right)\rho^{1/2} u^{1/2} k^{1/2} C_p^{\ 1/2} . \tag{25}$$

It is assumed that

$$\frac{k}{C_p \mu} = \frac{1}{Pr}$$

is constant, and that C_p itself is also constant.

The following mean and deviation quantities are considered:

$$\begin{aligned} R_a &= \overline{R_a} + r_a' & \rho &= \overline{\rho} + \rho' \\ k &= \overline{k} + k & E &= \overline{E} + e' \\ u &= \overline{u} + u' \end{aligned} \tag{26}$$

Substitution of Equations 26 into 25 yields

$$\frac{(\overline{E}+e')^2}{R_w(R_w-\overline{R}_a-r_a')} = (\frac{\pi \ell}{\alpha R_o} A)(\overline{k}+k') + (\frac{\pi \ell D}{\alpha R_o}^{1/2} \cdot [\frac{C_p}{Pr}]^{1/2} B)(\overline{\rho}+\rho')^{1/2}(\overline{u}+u')^{1/2}(\overline{k}+k')^{1/2} \qquad (27)$$

According to the Binomial Theorem,

$$\frac{(\overline{E}+e')^2}{R_w(R_w-\overline{R}_a)} \cdot \frac{1}{1-\frac{r_a'}{R_w-\overline{R}_a}} = \frac{(\overline{E}+e')^2}{R_w(R_w-\overline{R}_a)} \cdot (1+\frac{r_a'}{R_w-\overline{R}_a}). \qquad (28)$$

Note that

$$(\overline{E} = e')^2 \simeq \overline{E}^2 + 2\overline{E}e' . \qquad (29)$$

Using Equations 28 and 29 for the left side of 27, and expanding the right side of 27, and neglecting small quantities yields:

$$\frac{\overline{E}^2}{R_w(R_w-\overline{R}_a)} + \frac{E^2 r_a'}{R_w(R_w-\overline{R}_a)^2} + \frac{2\overline{E}e'}{R_w(R_w-\overline{R}_a)} = (\frac{\pi \ell}{\alpha R_o} A)(\overline{k}+k') + \qquad (30)$$

$$+ (\frac{\pi \ell D}{\alpha R_o}^{1/2} [\frac{C_p}{Pr}]^{1/2} B)(\overline{\rho u k} + \overline{\rho u}k' + \overline{\rho}u'\overline{k} + \rho'\overline{u}\,\overline{k})^{1/2} .$$

But

$$(\overline{\rho uk} + \overline{\rho u}k' + \overline{\rho}u'\overline{k} + \rho'\overline{uk})^{1/2} \simeq (\overline{\rho uk})^{1/2}(1+ \frac{1}{2}[\frac{k'}{k} + \frac{u'}{u} + \frac{\rho'}{\rho}]). \qquad (31)$$

Thus Equation 30 becomes

$$\frac{\overline{E}^2}{R_w(R_w-\overline{R}_a)} + \frac{\overline{E}^2 r_a'}{R_w(R_w-\overline{R}_a)^2} + \frac{2\overline{E}e'}{R_w(R_w-\overline{R}_a)} = \left(\frac{\pi\ell}{\alpha R_o} A\right)(\overline{k} + k') + \tag{32}$$

$$+\left(\frac{\pi\ell D}{\alpha R_o}\right)^{1/2} \left[\frac{C_p}{Pr}\right]^{1/2} B)\,(\overline{\rho uk})^{1/2}\left(1 + \frac{1}{2}\left[\frac{k'}{k} + \frac{u'}{u} + \frac{\rho'}{\rho}\right]\right).$$

The time average form of Equation 32 is

$$\frac{\overline{E}^2}{R_w(R_w-\overline{R}_a)} = \left(\frac{\pi\ell}{\alpha R_o} A\right)\overline{k} + \left(\frac{\pi\ell D}{\alpha R_o}\right)^{1/2} \left[\frac{C_p}{Pr}\right]^{1/2} B)\,(\overline{\rho uk})^{1/2}. \tag{33}$$

Subtraction of Equation 33 from 32 gives

$$\frac{\overline{E}^2 r_a'}{R_w(R_w-\overline{R}_a)^2} + \frac{2\overline{E}e'}{R_w(R_w-\overline{R}_a)} = \left(\frac{\pi\ell}{\alpha R_o} A\right)k' + \tag{34}$$

$$+\left(\frac{\pi\ell D}{\alpha R_o}\right)^{1/2} \left[\frac{C_p}{Pr}\right]^{1/2} B)\,\frac{(\overline{\rho uk})^{1/2}}{2}\left(\frac{k'}{k} + \frac{u'}{u} + \frac{\rho'}{\rho}\right).$$

The following relationships are known:

$$r_a' = R_o\,\alpha\,t' \qquad k' = nt' \qquad \rho' = -\overline{\rho}\,\frac{t'}{T_a} \tag{35}$$

Thus Equation 34 becomes

$$\frac{\overline{E}^2 R_o \alpha}{R_w(R_w-\overline{R}_a)^2}\,t' + \frac{2\overline{E}}{R_w(R_w-\overline{R}_a)}\,e' = \left(\frac{n\pi\ell}{\alpha R_o} A\right)t' + \tag{36}$$

$$+ \left(\frac{\pi\ell D}{\alpha R_o}\right)^{1/2} \left[\frac{C_p}{Pr}\right]^{1/2} B)\,\frac{(\overline{\rho uk})^{1/2}}{2}\left(n\,\frac{t'}{k} - \frac{t'}{T_a} + \frac{u'}{\overline{u}}\right).$$

Since $n\,\frac{t'}{\overline{k}} - \frac{t'}{\overline{T}_a} << \frac{u'}{\overline{u}}$, Equation 36 becomes

$$\left[\frac{2\bar{E}}{R_w(R_w-\bar{R}_a)}\right] e' = \left[\frac{\pi \ell D^{1/2} C_p^{1/2} B \rho^{1/2} k^{1/2}}{2\alpha R_o \, Pr^{1/2} \, \bar{u}^{1/2}}\right] u' +$$

$$+ \left[\frac{n\pi\ell A}{\alpha R_o} - \frac{\bar{E}^2 R_o \alpha}{R_w(R_w-R_a)^2}\right] t'. \tag{37}$$

Equation 37 may be written

$$e' = \left[\frac{R_w(R_w-\bar{R}_a)\pi \ell D^{1/2} C_p^{1/2} B \bar{\rho}^{1/2} \bar{k}^{1/2}}{4 \bar{E} \alpha R_o \, Pr^{1/2} \, \bar{u}^{1/2}}\right] u' +$$

$$+ \left[\frac{R_w(R_w-\bar{R}_a) n\pi\ell A}{2 \bar{E} \alpha R_o} - \frac{\bar{E} R_o \alpha}{2 (R_w-\bar{R}_a)}\right] t'. \tag{38}$$

The coefficient of u' represents the sensitivity to velocity fluctuations, and the coefficient of t' represents the sensitivity to temperature fluctuations. These sensitivities could in principle be calculated, since all factors are either measurable quantities, physical properties, or known constants. In practice, however, this calculation yields values of the sensitivities that do not agree with those determined by actual calibration. This discrepancy is due to two of the supposedly known quantities in Equation 38, namely α and B. King's value for B, since it is based on his potential flow assumption, is seriously in error. The value of α found in tables of physical properties may also be in error because the value of α applicable to the wire in use depends very strongly on the history of that wire. In addition, contamination of the wire changes the value of D, the wire diameter, and the wire length ℓ is some

effective length rather than the actual length. Thus it is impossible to accurately determine the sensitivities by direct calculation. Instead the sensitivities are determined by calibration.

Although the expressions for the sensitivities in Equation 38 do not provide quantitative information, they do indicate the direction of variation in the sensitivities as various parameters are changed. Thus, the velocity sensitivity should decrease with increasing velocity, but velocity should not affect the temperature sensitivity to first order. The velocity sensitivity should increase with increasing wire temperature (resistance).

In order to determine the effect of parameter variation on the temperature sensitivity, further consideration of the two terms that comprise it is necessary. Equation 8 shows that, all other parameters remaining constant, an increase in T_a (i.e. a positive t') requires a decrease in E^2 (i.e. a negative e') in order to maintain the equality. Thus, the overall sign of the temperature sensitivity must be negative. Since all factors are inherently positive, this implies that

$$\frac{\bar{E} R_o \alpha}{2(R_w - \bar{R}_a)} > \frac{R_w (R_w - \bar{R}_a)\, n \pi \ell A}{2 \bar{E} \alpha R_o} \quad . \qquad (39)$$

Thus an increase in $\frac{\bar{E} R_o \alpha}{2(R_w - R_o)}$ causes an increase in the magnitude of the temperature sensitivity, and an increase in $\frac{R_w (R_w - \bar{R}_a) n \pi \ell A}{2\bar{E} \alpha R_o}$ causes a decrease.

Equation 33 shows that the quantity $\frac{\bar{E}^2}{R_w (R_w - R_a)}$ is independent of $T_w - \bar{T}_a$. That is if the parameter $T_w - \bar{T}_a$ is varied,

$\dfrac{\bar{E}^2}{R_w(R_w - \bar{R}_a)}$ remains constant. Further if $\bar{R}_a$ is constant, $\bar{E}^2$ is proportional to R_w^2. Now

$$\frac{\bar{E}\, R_o\, \alpha}{2\,(R_w - \bar{R}_a)} = \frac{R_w}{\bar{E}} \; \frac{\bar{E}^2}{R_w(R_w - \bar{R}_a)} \; \frac{\alpha\, R_o}{2}, \tag{40}$$

and

$$\frac{R_w(R_w - R_a)\, n\pi\ell A}{2\,\bar{E}\,\alpha\, R_o} = \bar{E}\; \frac{R_w(R_w - R_a)}{\bar{E}^2} \; \frac{n\pi\ell A}{R_o\,\alpha}. \tag{41}$$

Since $\dfrac{R_w}{\bar{E}}$ and $\dfrac{\bar{E}^2}{R_w(R_w - \bar{R}_a)}$ are independent of $T_w - \bar{T}_a$, it follows from Equation 40 that variation of $T_w - \bar{T}_a$ has no effect on $\dfrac{\bar{E}\, R_o\, \alpha}{2(R_w - \bar{R}_a)}$ to first order. Similarly it follows from Equation 41 that $\dfrac{R_w(R_w - R_a)\, n\pi\ell A}{2\,\bar{E}\,\alpha\, R_o}$ increases linearly with increasing $T_w - \bar{T}_a$. As previously shown, an increase in this term causes a decrease in temperature sensitivity. Thus an increase in $T_w - \bar{T}_a$ causes a decrease in temperature sensitivity. Thus it appears that velocity fluctuations could be measured directly by operating at very high temperature differences and that temperature fluctuations could be measured directly by operating at very low temperature differences.

If consideration is given to changing the dimensions and material of the wire, further effects on the sensitivities occur. Velocity sensitivity increases with wire length while the temperature sensitivity decreases. An increase in wire diameter causes an increase in velocity sensitivity and no change in temperature sensitivity to first order. An increase in temperature coefficient causes a decrease in velocity sensitivity and an increase in temperature sensitivity.

Once the desired information on trends in sensitivity is recognized, it is convenient to resort to a more compact notation:

$$S_u = \frac{R_w(R_w - R_a)\pi \ell D^{1/2} C_p^{1/2} B\, \bar{k}^{1/2} \bar{\rho}^{1/2}}{4\, \bar{E} \alpha R_o P_r^{1/2} \bar{u}^{1/2}} \tag{42}$$

and

$$S_t = \frac{\bar{E} R_o \alpha}{2(R_w - \bar{R}_a)} - \frac{R_w (R_w - \bar{R}_a) n \ell A \pi}{2\, \bar{E} \alpha R_o} . \tag{43}$$

thus Equation 38 becomes

$$e' = S_u u' - S_T t' . \tag{44}$$

Squaring and time averaging yields

$$\overline{e'^2} = \overline{S_u^2} - 2 S_u S_T \overline{u't'} + S_T^2 \overline{t'^2} . \tag{45}$$

The sensitivities S_u and S_T must be determined from calibration. This is discussed in the section on procedure. The quantity, $\overline{e'^2}$,

is experimentally measured. From known values of $\overline{e'^2}$, S_u, and S_T, a set of simultaneous equations of the form of Equation 39 can be formed. This set can then be solved for $\overline{u'^2}$, $\overline{u't'}$, and $\overline{t'^2}$. This solution is discussed in the RESULTS section.

APPARATUS

Flow System

The flow system is shown schematically in Figure 1. A Craftsman Model 315.16970, 3HP industrial vacuum cleaner was operated as a blower to supply air to the system. A three inch galvanized duct carried the air to the highest point of the flow system where the duct tapered to meet the 1.0625 inch inside diameter Type M copper tubing that comprised the remainder of the loop. The three-inch duct was fitted with a bleed line and damper. The flow rate in the loop could be varied by using the damper to alter the division of air between loop and bleed line. Above the bleed line in the duct was an orifice meter for measuring air flow rate in the loop. (The calibration curve for the orifice meter is given in Appendix B.) In the copper tube, the air passed downward through an 83 inch unheated velocity developing section. This was followed by a 58 inch heating section which was wound with nichrome heating wire and covered with 1.125 inches of pre-formed pipe insulation. Probes were inserted upward into the copper tube as shown. All measurements were made in the end plane of the heating section.

Iron-constantan bulk thermocouples were installed at the beginning of the velocity developing section and at the end of the heating section, and wall thermocouples were installed at the end of the heating section.

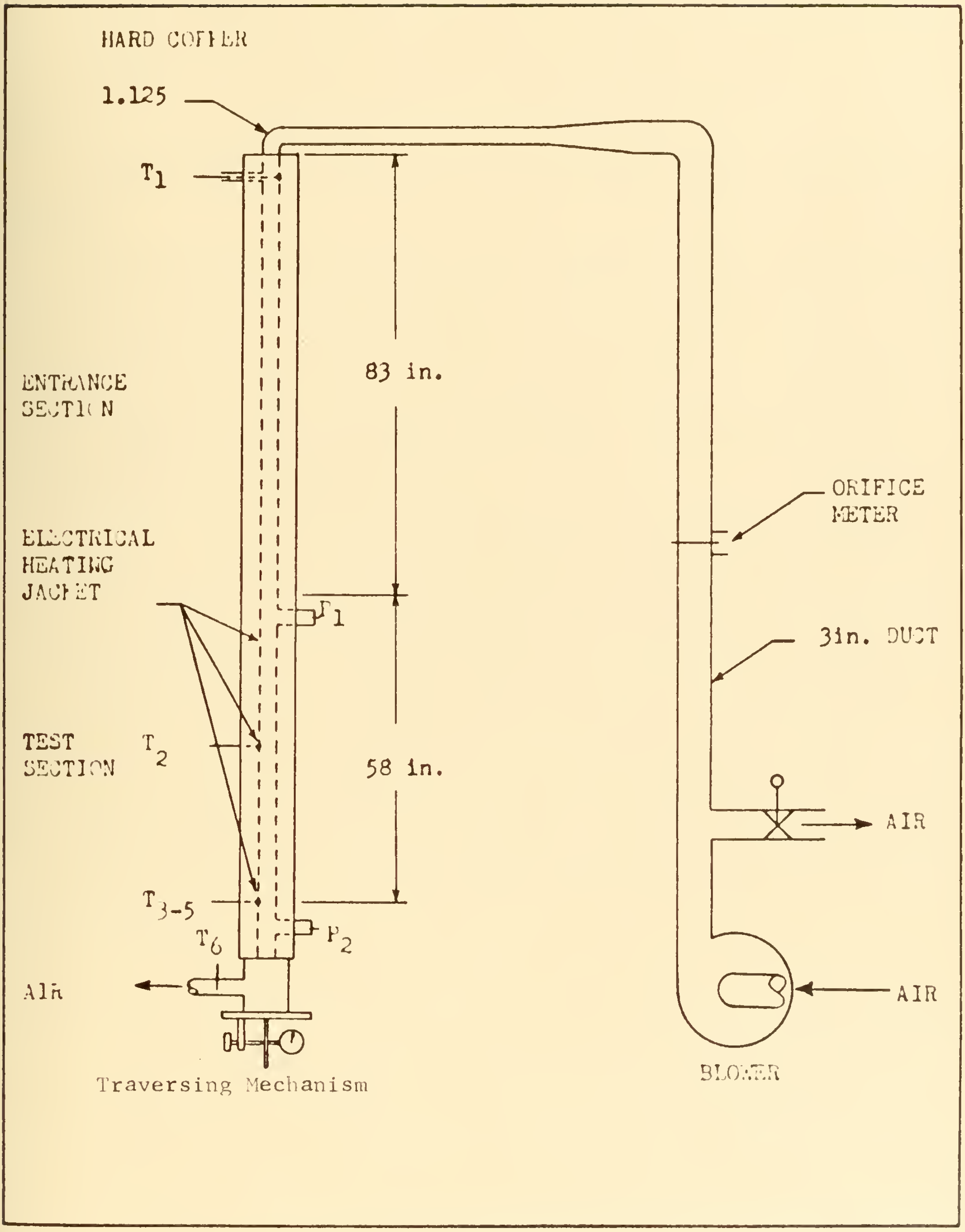

Figure 1. Flow Diagram of Apparatus

Probes and Traversing Mechanisms

The rapid response thermocouple used (a Heat Technology Laboratory TCFW 202-ChA-5) is shown in Figure 2. The response time of this thermocouple has been estimated by Rodriguez-Ramirez to be 5 milli-seconds.

The hot-wire probe used (a Thermo Systems 1210-T1.5) is shown in Figure 3.

Positioning of the rapid response thermocouple was by means of the traversing mechanism shown in Figure 4. When in place as shown in Figure 1 the mechanism was, of course, inverted. The ball joint permitted radial movement of the probe across the tube. Radial position was measured with the dial guage shown.

Figure 5 shows the traversing mechanism used to position the hot-wire in the loop. This traversing mechanism replaced the thermocouple traversing mechanism at the bottom of the loop when hot-wire measurements were being made. The upper block in Figure 5 could be moved laterally so as to place the hot-wire probe at the desired radial position, while the lower plate shown in Figure 5 was bolted to the loop. A pitot tube and a local mean thermocouple were inserted through the auxiliary probe entrances.

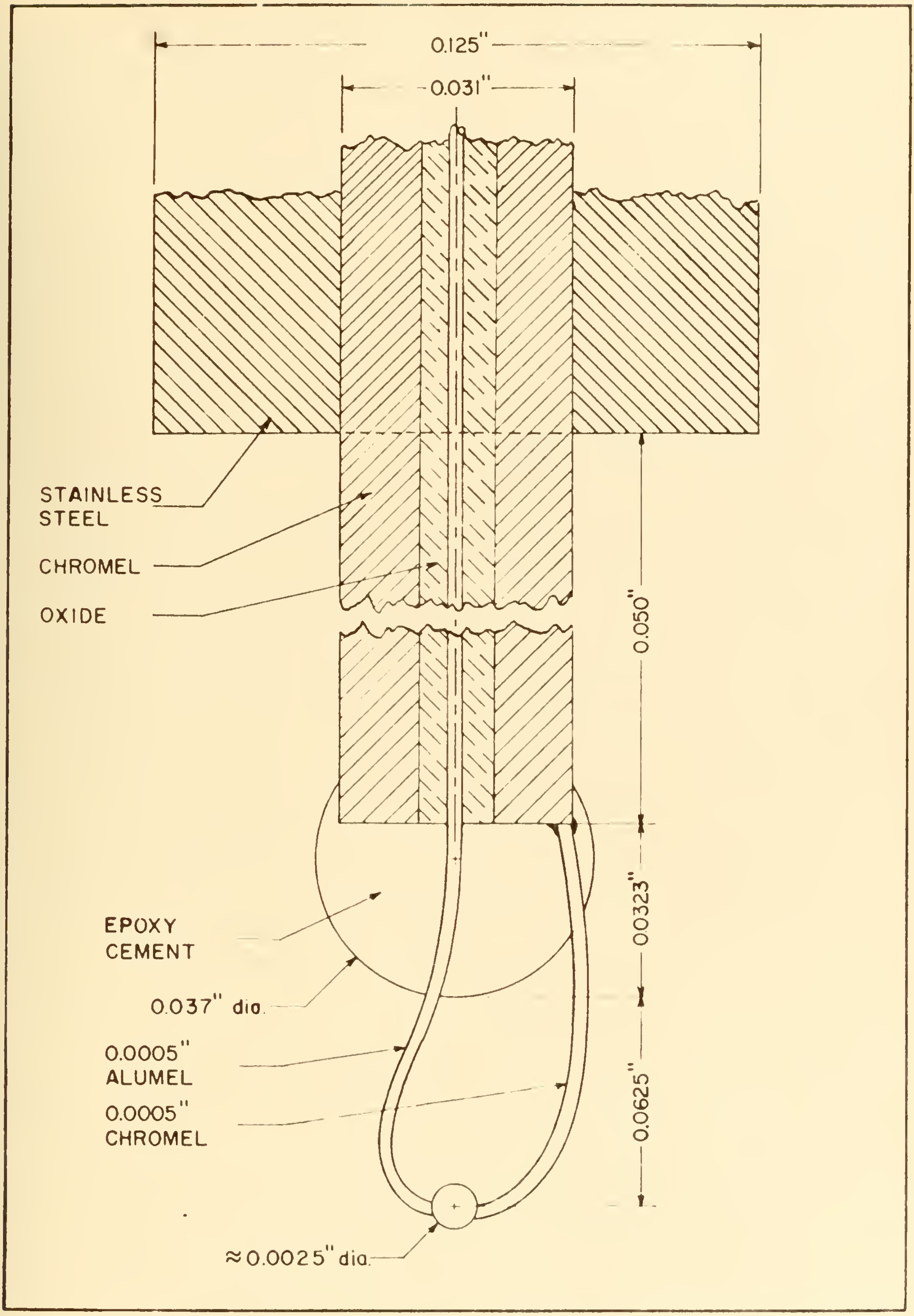

Figure 2. Fast Response Thermocouple

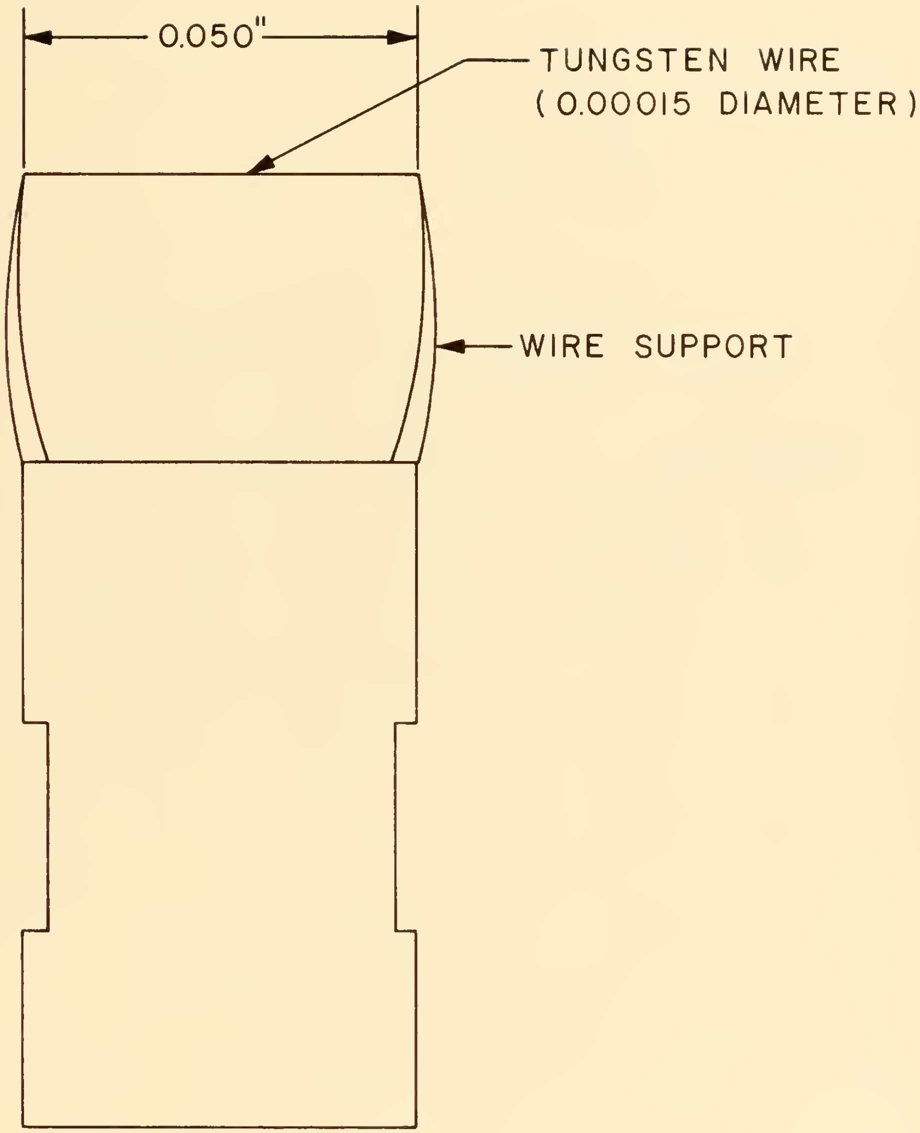

Figure 3. The Hot-Wire Probe

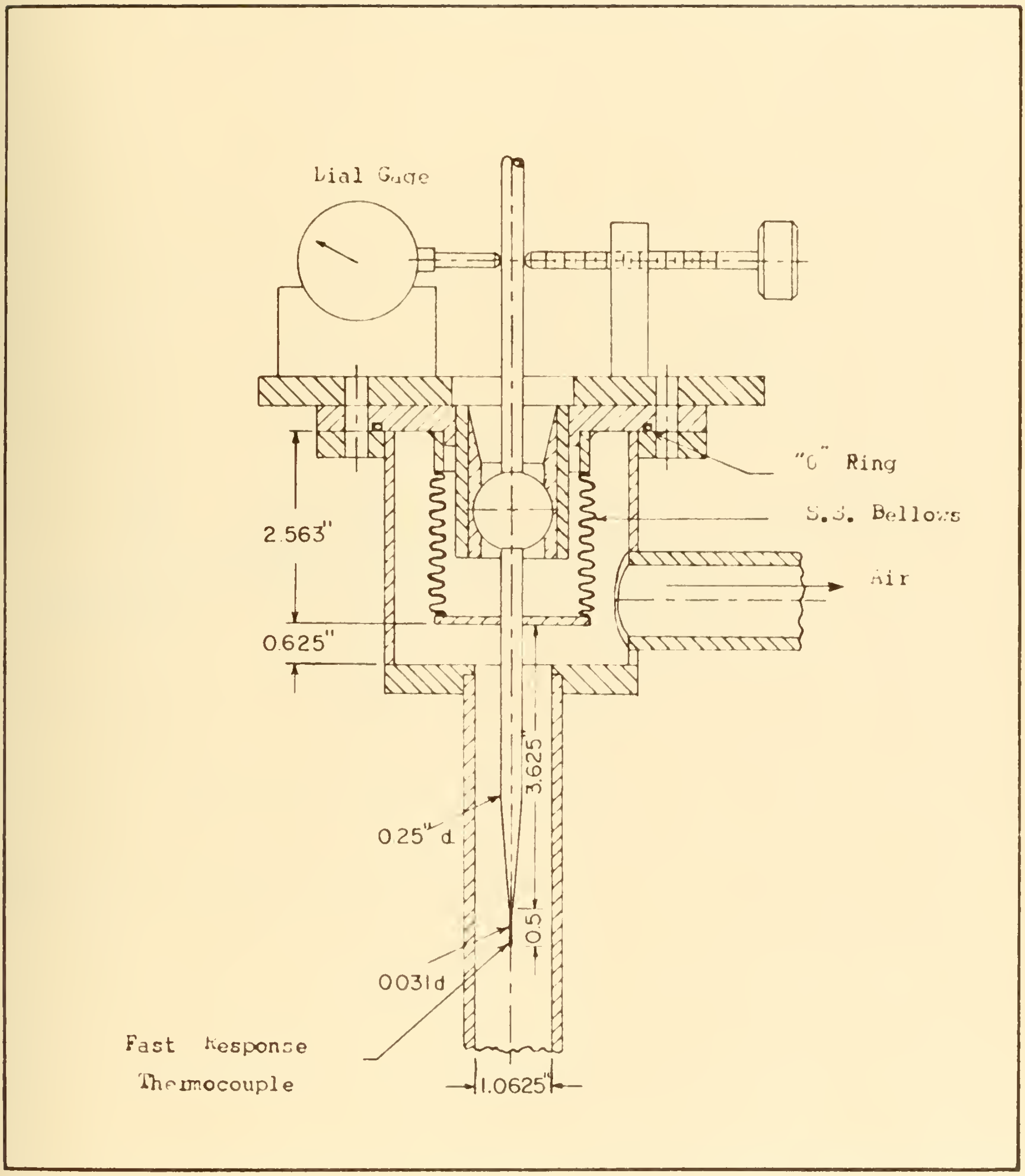

Figure 4. Thermocouple Traversing Mechanism

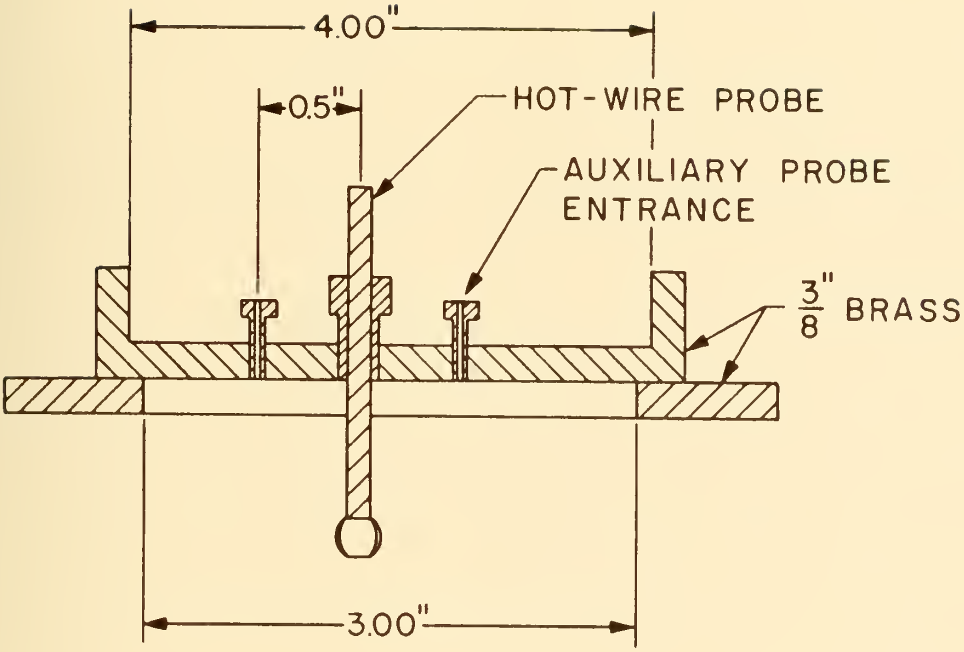

Figure 5. Hot-Wire Traversing Mechanism

Instrumentation

Instrumentation for hot-wire measurements consisted of a Thermo Systems Type 1010 anemometer, and a Ballantine Model 320A True Root-Mean-Square Electronic Voltmeter.

For rapid-response thermocouple measurements, instrumentation consisted of a Tektronix 122 Amplifier (See Appendix C for frequency response.) and the Ballantine Voltmeter.

Bulk and wall thermocouple measurements were made with a Dana Model 2850 D.C. amplifier and a Beckman Model 4011R digital voltmeter.

PROCEDURE

Hot-wire in Isothermal Flow

The first step was calibration. The constant C defined by Equation 17 and appearing in Equation 18 can be determined from mean voltage and velocity measurements. It is seen from Equation 14 that if $\frac{\bar{E}^2}{R_w(R_w - R_a)}$ were plotted as a function of $\bar{u}^{\frac{1}{2}}$, the result should be a straight line with slope C.

The Calibration of the hot-wire probe was carried out with the probe in place in the loop and located at the tube centerline. Variation of $\bar{u}$ was achieved by varying the flow rate in the loop using the bleed line damper. The quantity $\bar{E}$ was measured at seven or eight different flow rates. The value of $\bar{u}$ at the centerline corresponding to each flow rate was measured with a pitot tube. The data were plotted as indicated above, a straight line was fitted to the points, and the slope was measured. Calibration curves are shown in Appendix E.

The second step was the making of fluctuation measurements. Equation 18 gives the relationship between the rms velocity fluctuation and the rms voltage fluctuation.

. The flow system was operated at Reynolds Numbers of 30,700, 41,500, and 49,800. For each Reynolds Number, measurements were made of $\sqrt{\overline{e'^2}}$ at eight points between the center and the wall of the tube corresponding to r/R of 0, 0.125, 0.250, 0.375, 0.500, 0.625, 0.750 and 0.875. A

pitot tube was used to measure $\bar{u}$ at the same points.

After all fluctuation measurements had been made, the calibration procedure was repeated to make certain that the constant C had not changed during the run.

Rapid Response Thermocouple in Non-Isothermal Flow

The flow was adjusted so that the Reynolds Numbers in this part were the same as those in the previous section. The applied heating was 430 watts in all cases.

Measurement was made of $\sqrt{\overline{e'^2}}$ from the rapid response thermocouple as a function of radial position for each Reynolds Number. No calibration was done, since the constant, a, in Equation 24 was assumed to be that found in standard thermocouple tables[13]. This assumption is of questionable validity.

A conventional thermocouple was used to measure the centerline temperature, and the wall thermocouples were used to measure the wall temperature for each Reynolds Number.

Hot-Wire in Non-Isothermal Flow

The procedure of calibration and measurement outlined below represents one of the contributions of this work. It is anticipated that this procedure will be used for the glycol and mercury measurements previously mentioned.

As shown in the THEORETICAL BACKGROUND section, the sensitivities S_u and S_T depend on two parameters: $\bar{u}$ and $T_w - \bar{T}_a$. Thus, in calibration it is necessary to determine the functional dependence on each parameter.

Calibration for temperature sensitivity was also carried out with

the probe in place and at the tube centerline. Velocity variation was again achieved by use of the bleeder line damper, and $\bar{u}$ was measured with a pitot tube. In this way five different values of $\bar{u}$ were used, and for each value of $\bar{u}$ thirteen values of $T_w-\bar{T}_a$ were used.

These data were plotted as $\bar{E}$ versus $\bar{u}$ for constant values of $T_w-\bar{T}_a$ and as $\bar{E}$ versus $T_w-\bar{T}_a$ for constant values of $\bar{u}$. These curves are shown in Appendix G. The sensitivities S_u and S_T are the derivatives of these curves. These derivatives were obtained from analytical differentiation of parabolas fitted to the data by the method of least squares. The selection of parabolas is arbitrary, but the relatively slow and smooth variation of the data makes a parabola a satisfactory approximation.

Note that $T_w-\bar{T}_a$ must be computed from measurements made of $R_w-\bar{R}_a$. The resistance-temperature characteristic of the hot-wire probe was experimentally determined to be as shown in Appendix D.

Once S_u and S_T were known as functions of $\bar{u}$ and $T_w-\bar{T}_a$, fluctuation measurements were made. The rms voltage fluctuation was measured at $r/R = 0$ and $r/R = .5$ for each flow rate and temperature difference considered in calibration.

When all fluctuation measurements had been completed, the calibration was repeated to determine the drift in S_u and S_T.

RESULTS

Hot-Wire in Isothermal Flow

Figure 6 shows the axial turbulent intensity at the centerline of the pipe compared with the work of Sandborn.[11]

Figure 7 shows axial turbulent intensity as a function of radial position for three different Reynolds Numbers compared with the work of Laufer.[10]

The agreement of present results with those of Sandborn[11] and Laufer[10] is rather good. The data used by Sandborn to obtain his correlation show a scatter of ± 10 percent. The results of the present work are well within this range.

Rapid Response Thermocouple in Non-Isothermal Flow

Figure 8 shows the temperature fluctuation intensity as a function of radial position. Rodriguez-Ramirez[14], and also Tanimoto and Hanratty[15] have published results of this nature. The present results are for a range of Reynolds Numbers higher than the range considered by Rodriguez-Ramirez; however, a preliminary run was made in which the flow rate and heat input were the same as those in one of Rodriguez-Ramirez' runs. The results of this run deviated from those of Rodriguez-Ramirez by less than 5 percent. The temperature gradients used by Tanimoto and Hanratty were so much larger than those used in the present work that comparison is not possible.

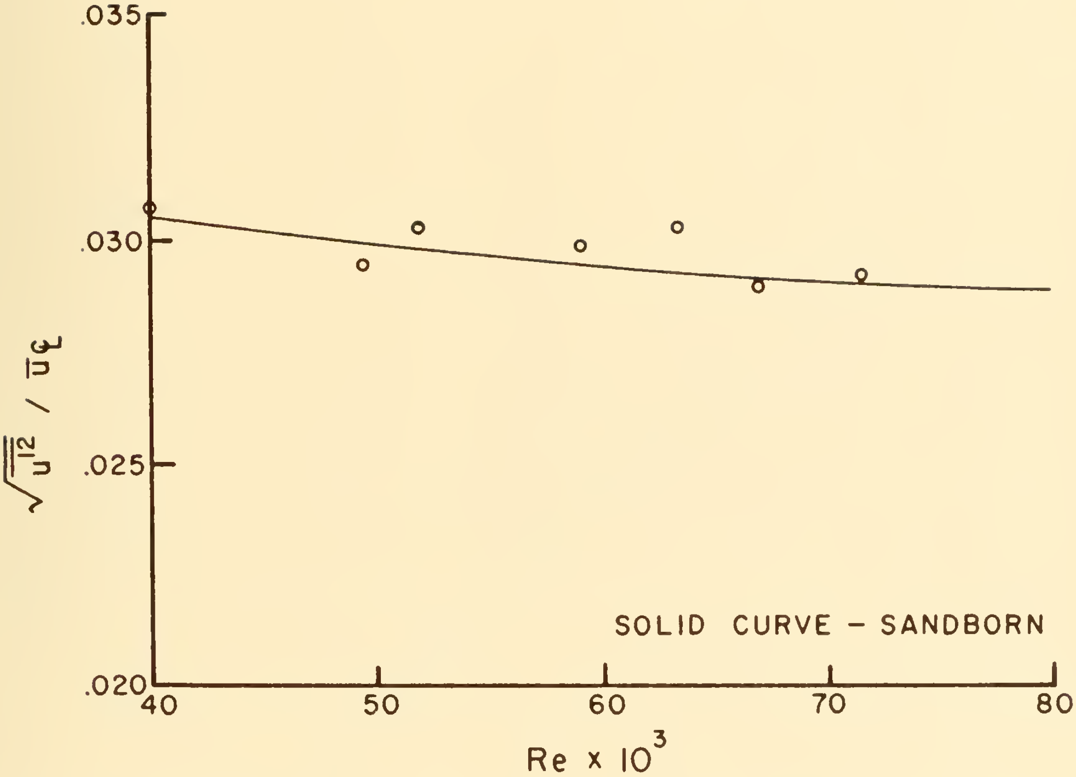

Figure 6. Centerline Velocity Turbulence Intensity in Air

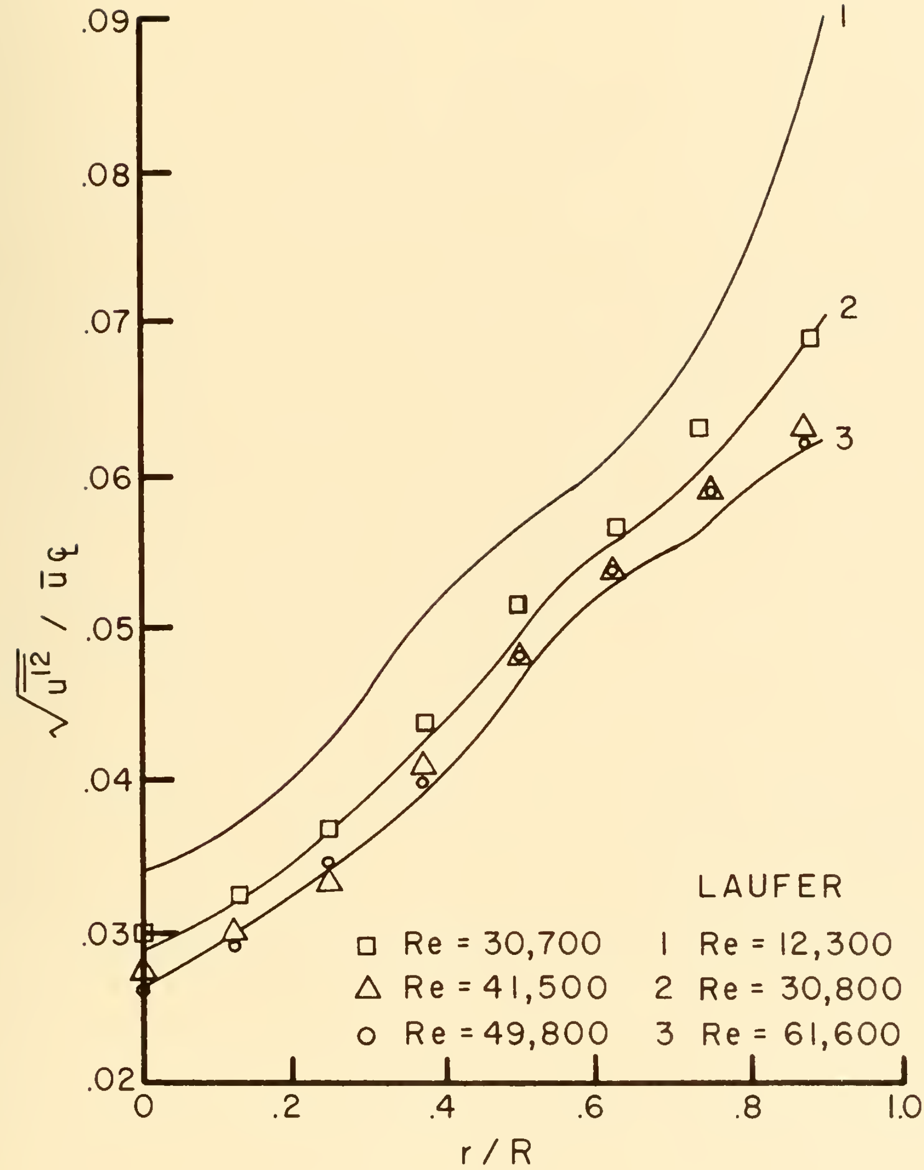

Figure 7. Velocity Turbulence Intensity in Air I

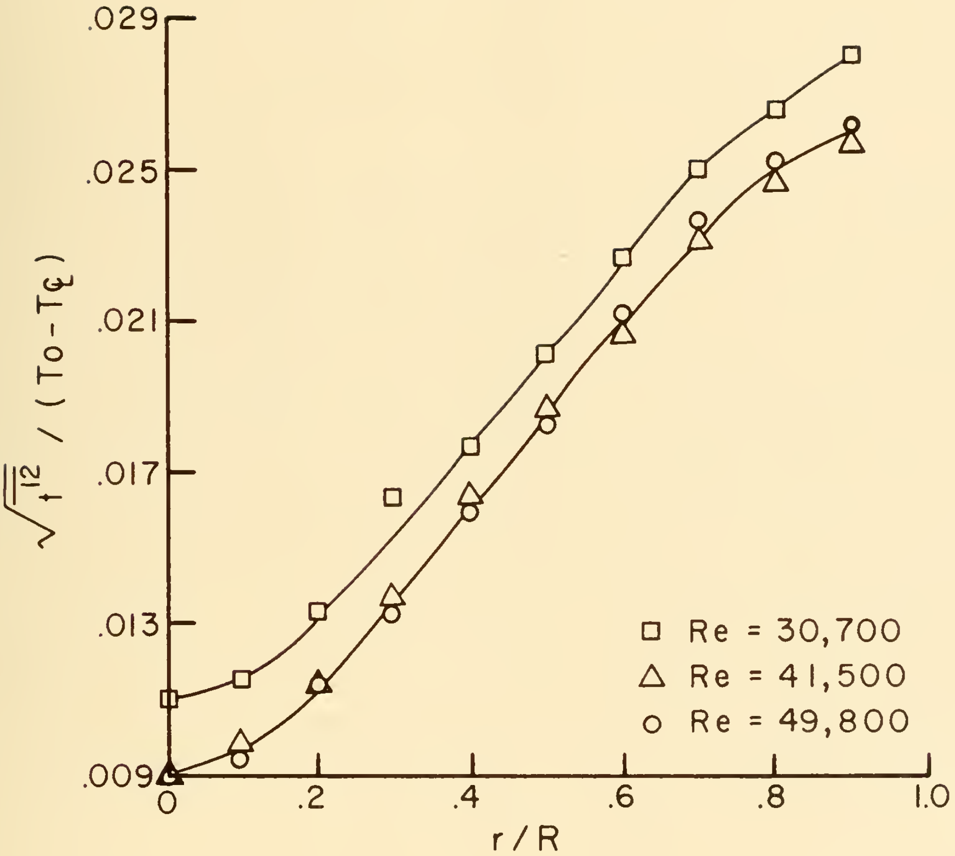

Figure 8. Temperature Turbulence Intensity in Air

Hot-Wire in Non-Isothermal Flow

Figures 9 and 10 show the dependence of the sensitivities S_u and S_T on the parameters $\bar{u}$ and $T_w - \bar{T}_a$. The velocity sensitivity, S_u, increases with increasing temperature difference and decreases with increasing velocity as predicted from Equation 38. The temperature sensitivity decreases with increasing temperature difference as predicted from Equation 38. Note that there is a secondary dependence on velocity not predicted by Equation 38. This dependence is due to the velocity dependence of the effective wire length.

The investigation of various calculating schemes including the selection of the best one for analyzing the non-isothermal data was an important part of the present work. As pointed out in the section on theoretical development, Equation 45 gives the relationship between the unknown quantities $\overline{u'^2}$, $\overline{u't'}$ and $\overline{t'^2}$ and the known quantities S_u, S_T, and $\overline{e'^2}$. Since there are three unknowns, at least three equations of the form of Equation 39 are needed. These can be obtained by operating the hot-wire at least three values of T_w (and hence of $T_w - \bar{T}_a$). For each value of $T_w - \bar{T}_a$, the values of S_u and S_T appropriate to the mean velocity, $\bar{u}$, of the flow are read from Figures 9 and 10, and $\overline{e'^2}$ is measured. Thus, for each value of $T_w - \bar{T}_a$ an equation is formed.

Once the set of equations is obtained, a number of methods of solution are available. The most obvious one is the simultaneous solution of three such equations by a method such as Gaussian reduction.[16] However, the numerical calculations involve the subtraction of large numbers whose difference is small, which has the effect of greatly magnifying the errors in the data. Since the errors in S_u and S_T were already large, the result was errors in the calculated values of $\overline{u'^2}$, $\overline{u't'}$, and $\overline{t'^2}$ of the

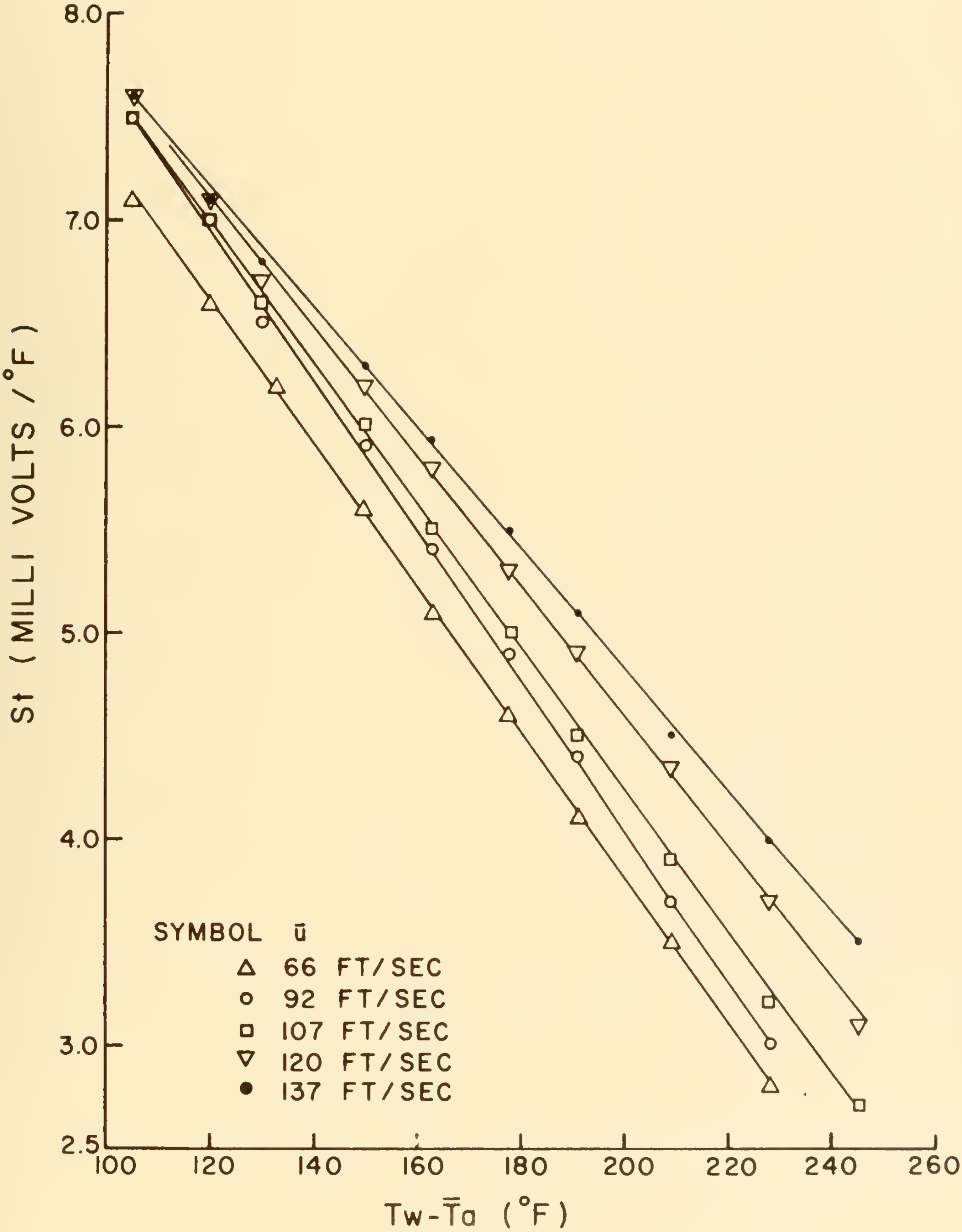

Figure 9. Hot-Wire Temperature Sensitivity

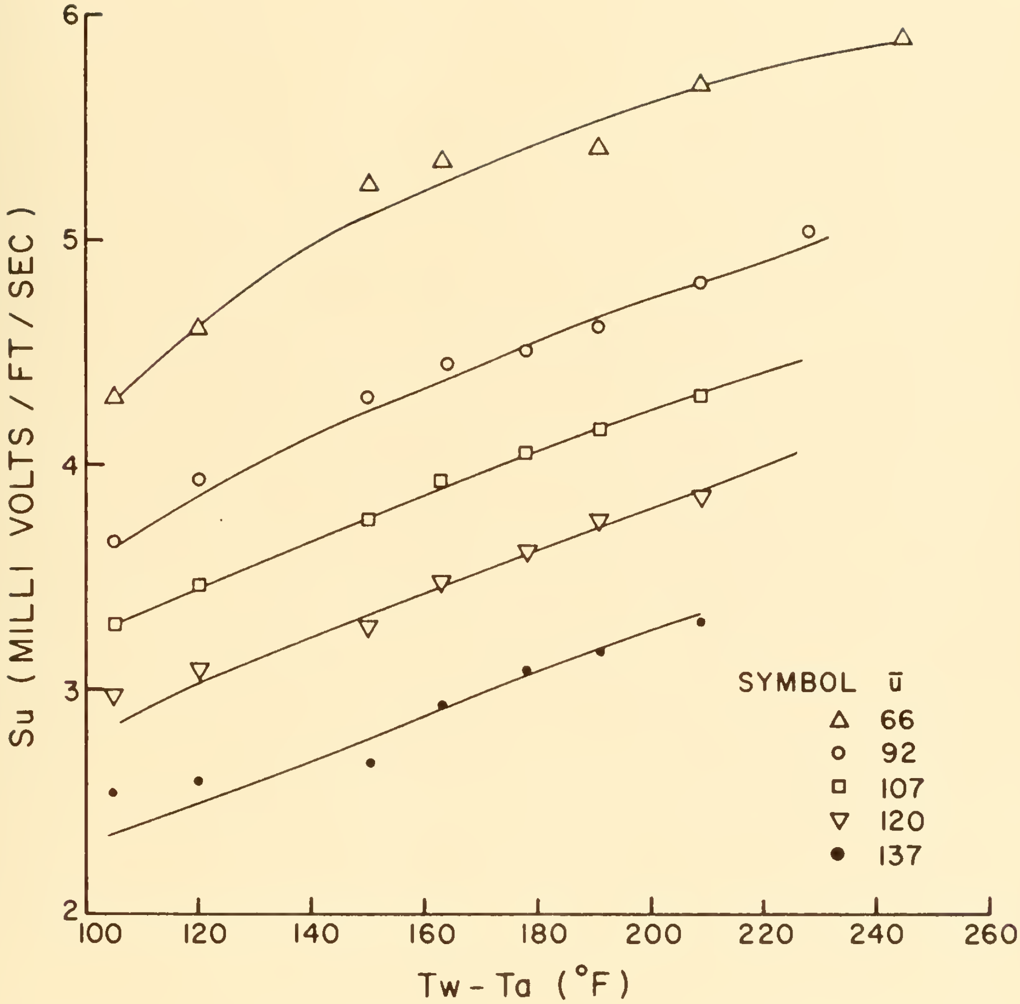

Figure 10. Hot-Wire Velocity Sensitivity

order of 500 percent.

The Kovasznay Fluctuation Diagram[17] is a graphical method of solving the set of equations in which equation 39 is divided by $S_T^{\,2}$ to give:

$$\frac{\overline{e'^2}}{S_T^{\,2}} = \left(\frac{S_u}{S_T}\right)^2 \overline{u'^2} - 2\left(\frac{S_u}{S_T}\right)\overline{u't'} + \overline{t'^2} . \tag{46}$$

Then the quantity $\dfrac{\overline{e'^2}}{S_T^{\,2}}$ is plotted versus $\dfrac{S_u}{S_T}$. Note that analytically the relationship between the two is described by a parabola. By the method of least squares a parabola is fitted to the data. The computer program used to do this fitting is listed in Appendix F. The intercept of this parabola with the $\dfrac{\overline{e'^2}}{S_T^{\,2}}$ axis is $\overline{t'^2}$, the slope at $\dfrac{S_u}{S_T} = 0$ is $- 2\overline{u't'}$, and the curvature of the parabola is $\overline{u'^2}$. This method was used on the present data, but the need to extrapolate the data from $\dfrac{S_u}{S_T}$ of some non-zero value to $\dfrac{S_u}{S_T} = 0$ and then determine the slope at $\dfrac{S_u}{S_T} = 0$ resulted in a large uncertainty in $\overline{u't'}$. This same problem was encountered by Arya and Plate[9], who suggested that if an independent measurement of $\overline{t'^2}$ could be obtained to locate the intercept of the curve accurately, then reliable values of the remaining two unknowns $\overline{u't'}$ and $\overline{u'^2}$ could be determined by the Kovasznay method. This procedure was followed with the present data. The value of $\overline{t'^2}$ used was the value found using the rapid response thermocouple. The results were still rather uncertain, but the uncertainty was less than for any of the other methods. (The Kovasznay Fluctuation Diagrams for representative cases are shown in Appendix H.)

The numerical values of $\sqrt{\overline{u'^2}}/\bar{u}_{\mathbb{C}}$ presented in Figures 11 and 12 deviate seriously from the isothermal results with which it is thought they should agree. (See, for instance Corrsin and Uberoi[5]) The trends

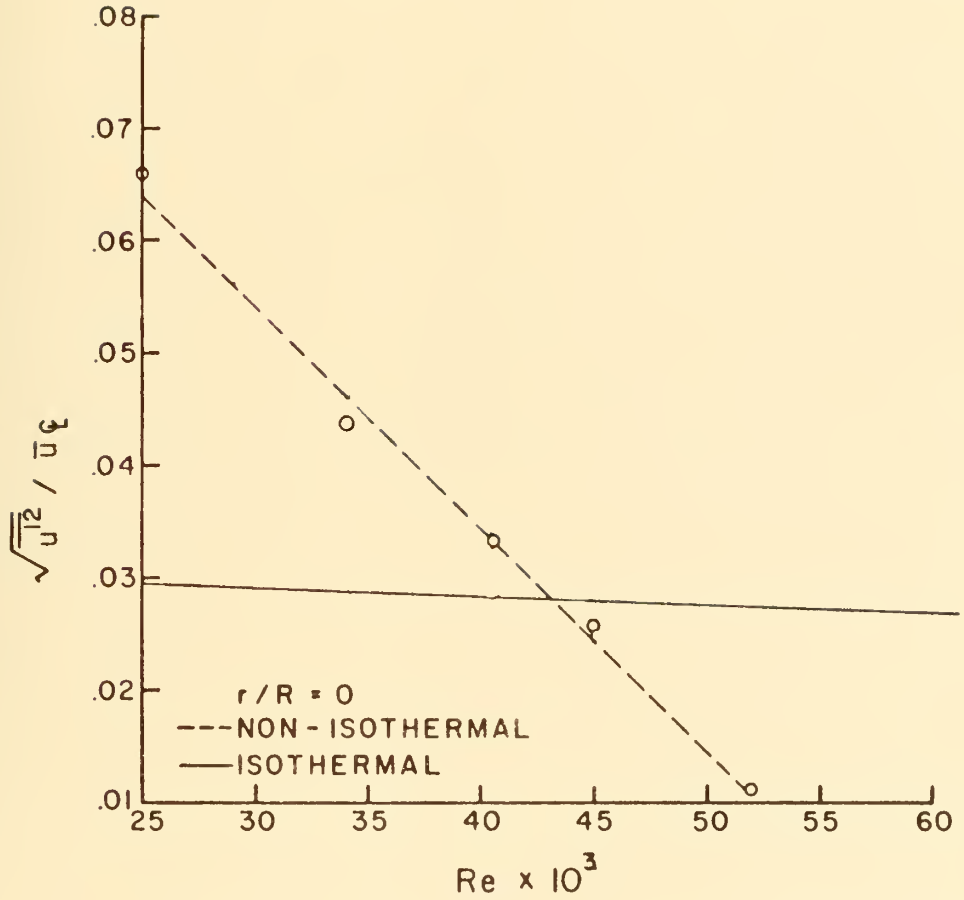

Figure 11. Velocity Turbulence Intensity in Air II

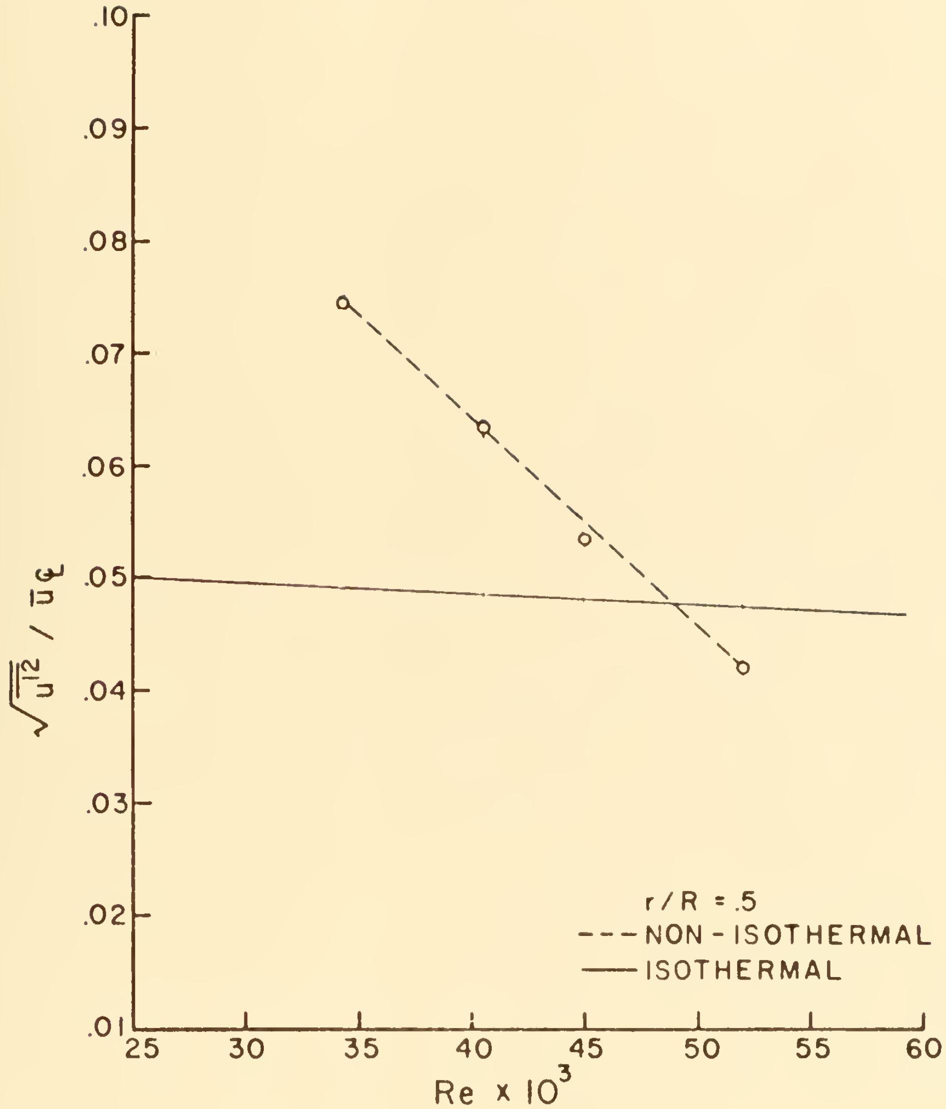

Figure 12. Velocity Turbulence Intensity in Air III

of the results with Reynolds Number and radial position are in accordance with expectations.

The calculated values of $\overline{u't'}/\bar{u}_{\mathrm{C\!L}}(T_o-T_{\mathrm{C\!L}})$ are presented in Figure 13. Turbulence at the centerline in pipe flow for the Reynolds numbers used in the present work should be isotropic. Thus $\overline{u't'}$ and $\overline{u't'}/\bar{u}_{\mathrm{C\!L}}(T_o-T_{\mathrm{C\!L}})$ should both be zero at the centerline. The centerline results in Figure 13 do not exhibit this behavior. However the error in these results is roughly estimated in Appendix I as 100%.

Away from the centerline the turbulence should no longer be isotropic, and $\overline{u't'}$ should no longer be zero. With heating from the wall as in the present case, $\overline{u't'}$, and hence $\overline{u't'}/\bar{u}_{\mathrm{C\!L}}(T_o-T_{\mathrm{C\!L}})$ should be negative. This trend is followed by the present results in that $\overline{u't'}/\bar{u}_{\mathrm{C\!L}}(T_o-T_{\mathrm{C\!L}})$ at $r/R = .5$ has a larger magnitude than at $r/R = 0$ and in that it has a negative sign. The quantity $\overline{u't'}/\bar{u}_{\mathrm{C\!L}}(T_o-T_{\mathrm{C\!L}})$ cannot continue to increase indefinitely as Reynolds Number increases, for this would mean no dissipation was taking place. The increasing trend in the results shown in Figure 13 for $r/R = .5$ is therefore not anticipated, but it is possible so long as the trend reverses itself at higher Reynolds Numbers. Arya and Plate[9] found that in the boundary layer growing on the wall of a wind tunnel $\overline{u't'}/\bar{u}_{\mathrm{C\!L}}(T_o-T_{\mathrm{C\!L}})$ remained nearly constant with increasing Reynolds Number. Again with an estimated error of 100 percent little significance can be attached to present results.

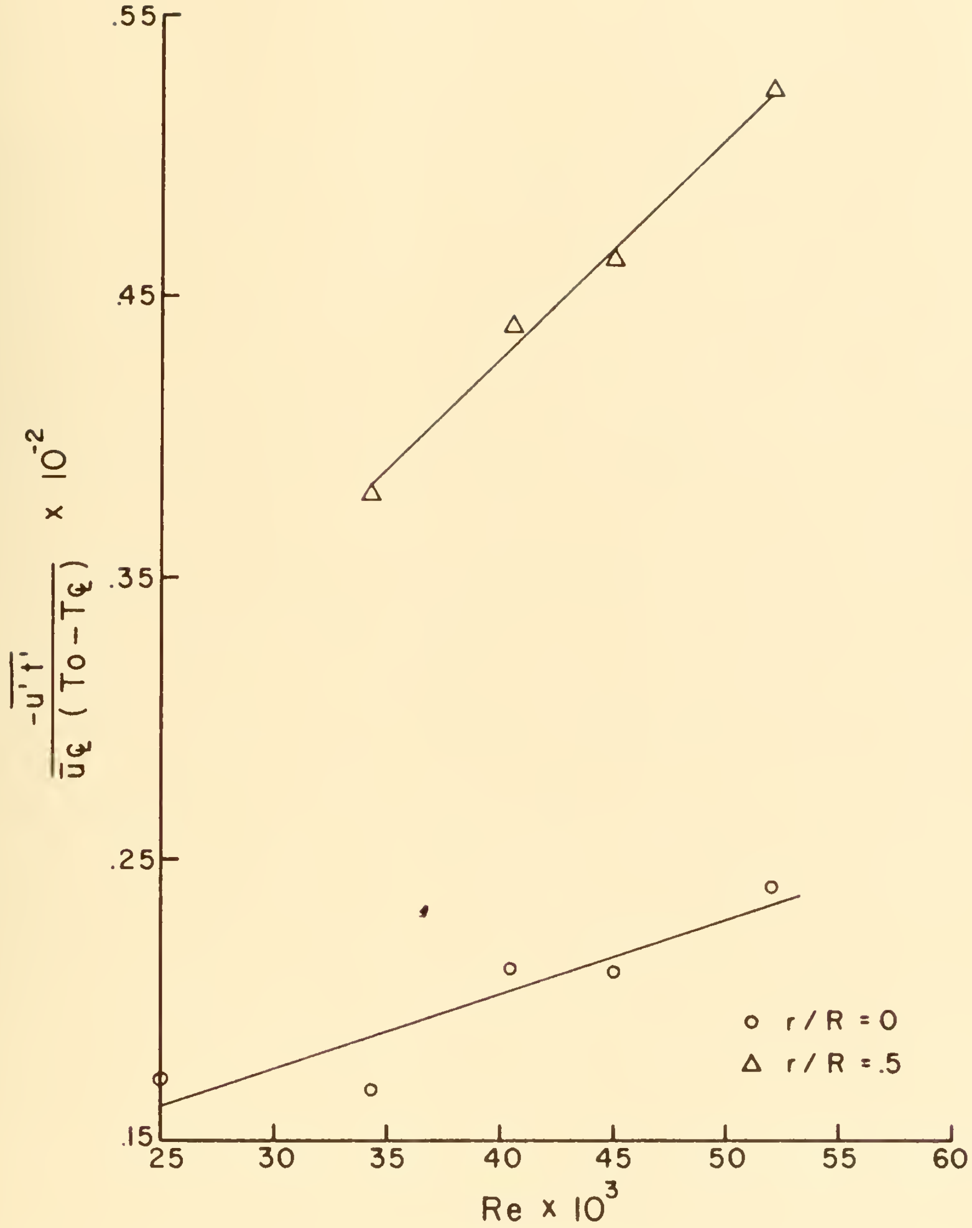

Figure 13. Temperature-Velocity Turbulence Intensity in Air

DISCUSSION

The numerical results for $\sqrt{\overline{u'^2}}/\bar{u}_{\text{Ł}}$ and $\overline{u't'}/\bar{u}_{\text{Ł}}$ are in general, too large. In view of the way in which these intensities are obtained from the Kovasznay Fluctuation Diagram, this suggests that S_u is too small. The temperature sensitivity S_T affects both coordinates in the same way, and therefore, errors in S_T would be self-compensating. However, errors in S_u affect only the $\frac{S_u}{S_T}$ coordinate. Too small a value of S_u would cause too large a slope and curvature in the fitted parabola and too large a value of $\overline{u'^2}$ and $\overline{u't'}$.

Because of the long time required for the system to come to thermal equilibrium after each change in flow rate, the data used to compute S_u for a given value of T_w-$\bar{T}_a$ were taken over a period of approximately eight hours. It is reasonable to expect an increase in the thickness of the layer of contamination on the wire during this period since the wire was continuously exposed to an inadequately filtered flow.

Kronauer[3] has shown that dirt accumulations on fine wires at low flow rates increase the heat transfer rate because the heat transfer area increases more rapidly than the heat transfer resistance as dirt accumulates. Thus, a dirty wire would require a higher value of $\bar{E}$ than a clean one to maintain it at a given temperature.

The wire used for the present measurements was examined under a microscope, and a significant amount of dirt was observed on it.

In the present calibration, $\bar{E}$ was measured at the highest calibration velocity first, and the velocity was decreased step by step until the lowest value was reached. As anticipated, $\bar{E}$ decreased with decreasing velocity, but the increasing layer of contamination apparently worked counter to this trend. Thus, in the calibration procedure used the rate of decrease of $\bar{E}$ was slower than if contamination had not been a problem. The result was a value of S_u that was too small.

Larger values of S_u would result in larger values of $\frac{S_u}{S_T}$ at the same value of $\frac{\overline{e'^2}}{S_T^2} - \overline{t'^2}$ on the Kovasznay Fluctuation Diagram and thus, a smaller slope and curvature of the fitted parabola. The calculated values of $\sqrt{\overline{\overline{u'^2}}}$ and $\overline{u't'}$ would then be smaller and in better agreement with the isothermal results.

It was not possible to determine the errors in $\sqrt{\overline{\overline{u'^2}}}$ and $\overline{u't'}$ caused by the drift in $\bar{E}$ noted above because it was not possible to measure what $\bar{E}$ would have been without contamination. Thus it was necessary to use a different method to estimate these errors. The method used is outlined in Appendix I, and the error estimates are 36 percent in $\sqrt{\overline{\overline{u'^2}}}$ and 100 percent in $\overline{u't'}$. As noted in Appendix I, these figures do not represent true confidence limits on the results. They are only rough estimates of the errors present.

The calibration curves for before and after as shown in Figures 24 through 26 show such a large drift that all data taken in between should be discarded. This was not done, since a number of attempts to obtain

better results failed. Note then, that all fluctuation intensities obtained from the present non-isothermal hot-wire measurements are of very doubtful reliability.

Due to inexperience in this area, a number of deviations from good experimental practice were present. First, although the wire was examined under a microscope after all measurements had been made, no examination was made before or during experimental runs. Thus the hypothesis of an increasing dirt layer cannot be verified. Second, no attempt was made to clean the wire during the course of experimental runs. Because of these errors it is not possible to analyze in detail or to correct for the drift that occurred.

In future work, provision should be made for careful filtration of the fluid and a means of rapid calibration to minimize drift. Two calibrations, one with increasing velocity and one with decreasing velocity, should be made to check for contamination. If it is still not possible to reduce drift to an acceptable level, provision should be made for the complete withdrawal of the probe from the flow.

A problem encountered with the present apparatus was difficulty in maintaining flow rate and heat input at desired levels. Long term temperature variations of two or three degrees persisted even after the system had come to "equilibrium". This was apparently caused by cycling of the room temperature.

The nature of the problems encountered in the present work serve as a guide in planning additional steps in the overall research program.

SUMMARY AND CONCLUSIONS

This work has developed procedures for the calibration of a hot-wire in non-isothermal flow. Further, the various calculation schemes available for analyzing non-isothermal flow fluctuation data have been evaluated and the Arya and Plate[9] modification of the Kovasznay Fluctuation Diagram[17] method has been found to be the most satisfactory.

Apparatus limitations and deviations from good experimental practice precluded the production of reliable numerical results.

The findings of this investigation are an important preliminary step in a comprehensive research program of non-isothermal flow measurements with hot-wire and hot-film anemometers.

BIBLIOGRAPHY

BIBLIOGRAPHY

1. Kovasznay, L.S.G., Calibration and Measurement in Turbulence Research by the Hot-Wire Method, NACA-TM-1130.

2. Kovasznay, L.S.G., Simple Analyses of the Constant Temperature Feedback Hot-Wire Anemometer, Report Aero/JHU (M-478), Johns Hopkins University, 1948.

3. Kronauer, Richard E., Survey of Hot-Wire Theory and Techniques, Pratt and Whitney Research Report No. 137, Pratt and Whitney Inc., 1953.

4. Corrsin, Stanley, Extended Uses of the Hot-Wire Anemometer-Velocity and Temperature Fluctuations, Report NACA TN 1864, National Advisory Committee for Aeronautics, 1949.

5. Corrsin, S. and Uberoi, M.S. NACA Report 998, 1950

6. Gibson, C. H., Chen, C. C., and Lin, S. C, "Measurements of Turbulent Velocity and Temperature Fluctuations in Wake of Sphere", AIAA Journal, 6:4, April 68, p 642-9.

7. Deissler, R., "Turbulent Heat Transfer and Temperature Fluctuations in a Field with Uniform Velocity and Temperature Gradients", International Journal of Heat and Mass Transfer, 6:4, April 63, p 257, 70.

8. Kunstman, Richard W., Non-Isothermal Turbulent Flow in Ducts, Ph.D. Thesis, University of Illinois, 1952.

9. Arya, S.P.S. and Plate, E.A., Hot-Wire Measurements of Turbulence in a Thermally Stratified Flow, Report CEM 67-SPSA-EJP11, Colorado State University, 1968.

10. Laufer, John, Investigation of Turbulent Flow in a Two Dimensional Channel, NACA Report 1053, National Advisory Committee for Aeronautics, 1951

11. Sandborn, V.A., Experimental Evaluation of Momentum Terms in Turbulent Pipe Flow, Report NACA 7N 3266, National Advisory Committee for Aeronautics, 1955.

12. King, Louis Vessot, "On the Convection of Heat from Small Cylinders in a Stream of Fluid: Determination of the Convection Constants of Small Platinium Wires with Applications to Hot-Wire Anemometry", Philosophical Transactions of the Royal Society, 214: 373-432 (1914).

13. Standard Conversion Tables for Leeds and Northrup Thermocouples, Leeds and Northrup Company, Philadelphia, Pennsylvania.

14. Rodriguez-Ramirez, Abraham, Characteristics of Turbulent Temperature Fluctuations in Air, M.S. Thesis, Purdue University, 1965.

15. Tanimoto, S. and Hanratty, T.J., "Fluid Temperature Fluctuations Accompanying Turbulent Heat Transfer in a Pipe", Chemical Engineering Science, 18: 307-311 (1963).

16. Scheid, Francis, Theory and Problems of Numerical Analysis, Schaum's Outline Series McGraw-Hill, New York, 1968.

17. Morkovin, M.V., Fluctuations and Hot-Wire Anemometry in Compressible Flows, AGARDograph 24, 1956.

18. Hinze, J.O., Turbulence, p. 1, McGraw-Hill, New York, 1959.

19. Beckwith, T.G. and Buck, N.L., Mechanical Measurements, Addison Wesley, Reading, Mass., 1961.

APPENDICES

APPENDIX A

APPENDIX A

TABLES OF EXPERIMENTAL DATA

Table 1

Orifice Meter Calibration

ΔP Orifice Meter (in)*	ΔP Pitot Tube At (in)*
4.553	2.173
3.151	1.595
2.172	1.123
1.114	0.571

* Manometer Fluid SPG. 0.797

Table 2

Tektronix Amplifier Frequency Response

Frequency (CPS)	Voltage in (Millivolts)	Voltage Out (Volts)
5	.200	.200
7	.200	.214
9	.200	.222
20	.200	.238
40	.200	.244
60	.200	.245
80	.200	.245
100	.200	.244
200	.200	.239
300	.200	2.31
400	.200	.226
500	.200	.217
600	.200	.210
700	.200	.200
800	.200	.193
900	.200	.185
1000	.200	.177
1100	.200	.170

Table 3

Calibration for Isothermal Re=49,800 Run

ΔP Pitot Tube (in of SPG.797 Fluid)	R_a (OHM)	R_w (OHM)	$\bar{E}$ (VOLTS)	$\sqrt{\overline{e'^2}}$ (MILLIVOLTS)
3.890	7.57	10.60	3.07	13.0
3.394	7.54	10.56	3.04	13.0
2.948	7.52	10.53	2.98	12.9
2.407	7.50	10.50	2.93	12.8
1.935	7.48	10.47	2.88	12.7
1.369	7.46	10.44	2.81	12.5
0.844	7.43	10.40	2.71	12.5
0.330	7.38	10.33	2.54	12.6
Before ↑				
4.004	7.57	10.60	3.08	----
0.737	7.42	10.39	2.70	----
After ↑				

Table 4

Data for Isothermal Re=49,800 Run

Radial Position (in)	ΔP Pitot Tube (in of SPG.797 Fluid)	$\bar{E}$ (Volts)	$\sqrt{\overline{e'^2}}$ (Millivolts)
0.0000	3.984	3.07	12.9
0.0625	3.964	3.07	12.9
0.1250	3.841	3.07	16.5
0.1875	3.691	3.06	19.5
0.2500	3.433	3.04	23.6
0.3125	3.184	3.02	27.5
0.3750	2.870	2.97	31.7
0.4375	2.411	2.94	36.4

Table 5

Calibration for Isothermal Re=30,700 and 41,500 Runs

ΔP Pitot Tube (in. of SPG.797 Fluid)	R_a (Ohms)	R_w (Ohms)	$\bar{E}$ (Volts)	$\sqrt{\overline{e'^2}}$ (Millivolts)
3.533	7.55	10.57	3.05	12.8
2.999	7.53	10.54	2.98	12.6
2.500	7.51	10.51	2.94	12.5
2.000	7.48	10.47	2.88	12.4
1.496	7.46	10.44	2.82	12.4
1.020	7.44	10.42	2.75	12.3
0.500	7.40	10.36	2.61	12.4
Before ↑				
2.780	7.52	10.53	2.96	----
1.020	7.44	10.42	2.75	
After ↑				

Table 6

Data for Isothermal Re=30,700 Runs

Radial Position (in.)	ΔP Pitot Tube (in.SPG.797 Fluid)	$\bar{E}$ (Volts)	$\sqrt{\overline{e'^2}}$ (Millivolts)
0.0000	1.480	2.81	12.2
0.0625	1.460	2.81	12.9
0.1250	1.400	2.80	15.1
0.1875	1.330	2.79	18.2
0.2500	1.240	2.78	21.9
0.3125	1.130	2.76	24.8
0.3750	1.020	2.74	28.6
0.4375	0.850	2.71	32.5

Table 7

Data for Isothermal Re=41,500 Run

Radial Position (in.)	ΔP Pitot Tube (in.SPG797 Fluid)	$\bar{E}$ (Volts)	$\sqrt{\overline{e'^2}}$ (Millivolts)
0.0000	2.780	2.95	12.4
0.0625	2.730	2.95	13.4
0.1250	2.630	2.95	15.6
0.1875	2.500	2.94	19.0
0.2500	2.330	2.92	22.6
0.3125	2.150	2.90	26.2
0.3750	1.960	2.89	29.4
0.4375	1.650	2.85	34.2

Table 8

Thermocouple Data for Re=30,700 Run

Radial Position (in)	0.00	0.05	0.10	0.15	0.20	0.25	0.30	0.35	0.40	0.45	NOISE
$\sqrt{\overline{e'^2}}$ (Milli-volts)	20.0	21.0	23.5	28.5	30.5	34.5	38.5	42.5	45.0	47.5	8.0

Table 9

Thermocouple Data for Re=41,500 Run

Radial Position (in)	0.00	0.05	0.10	0.15	0.20	0.25	0.30	0.35	0.40	0.45	NOISE
$\sqrt{\overline{e'^2}}$ (Milli volts)	15.0	15.7	18.3	21.5	25.0	28.5	32.0	35.5	38.0	39.5	6.0

Table 10

Thermocouple Data for Re=49,800 Run

Radial Position (in)	0.00	0.05	0.10	0.15	0.20	0.25	0.30	0.35	0.40	0.45	NOISE
$\sqrt{\overline{e'^2}}$ (Milli-volts)	12.0	12.8	14.8	17.5	20.5	24.0	27.0	30.0	32.0	33.2	3.0

Table 11

Non-Isothermal Hot-Wire "Before" Calibration Data

$R_w - \bar{R}_a$ (Ohm) ↓ / ΔP (in)* →	2.20	1.620	1.330	0.932	0.480
1.00	1.865	1.820	1.795	1.740	1.665
1.20	1.990	1.940	1.915	1.850	1.775
1.40	2.125	2.070	2.045	1.955	1.875
1.60	2.230	2.175	2.145	2.080	1.960
1.80	2.325	2.265	2.235	2.180	2.075
2.00	2.410	2.355	2.320	2.265	2.150
2.20	2.500	2.435	2.400	2.340	2.225
2.40	2.575	2.515	2.475	2.410	2.295
2.60	2.650	2.590	2.550	2.490	2.360
2.80	2.725	2.660	2.620	2.555	2.425
3.00	2.790	2.725	2.680	2.620	2.485
3.20	2.855	2.785	2.745	2.686	2.585
3.40	2.920	2.845	2.805	2.746	2.640

* Orifice Meter Manometer Fluid SPG 2.95

Table 12

Cold Resistances in "Before" Calibration

P (in.)*	R_{cold} (OHM)
2.120	7.42
1.620	7.46
1.330	7.49
0.932	7.57
0.480	7.80

Table 13

Temperature Difference Between Wall and Centerline

ΔP (in)*	$T_{r/R=1} - T_{r/R=0}$ ^oF
2.120	46
1.620	51
1.330	54
.932	61
.480	74

*Orifice Meter Manometer Fluid SPG 2.95

Table 14

Non-Isothermal Hot-Wire RMS Voltage Fluctuation Data for r/R=0

$R_w - \bar{R}_a$ (Ohm) ↓ \ ΔP (in)* →	2.120		1.620	1.330	0.932	0.480
1.00	24.8	Milli-volts	27.0	28.8	31.6	38.3
1.20	24.8		26.9	28.4	31.0	37.2
1.40	24.7		26.3	28.2	30.3	36.2
1.60	24.5		26.0	27.9	29.8	35.3
1.80	24.3		25.7	27.4	29.2	34.3
2.00	24.3		25.5	26.9	28.9	33.6
2.20	24.2		25.2	26.7	28.5	32.9
2.40	24.1		25.0	26.4	28.1	32.0
2.60	24.1		24.9	26.2	27.7	31.4
2.80	24.0		24.7	25.9	27.5	31.0
3.00	24.0		24.5	25.8	27.2	30.6
3.20	23.9		24.5	25.6	27.0	30.0
3.40	23.9		24.4	25.5	26.7	29.8

* Orifice Meter Manometer Fluid SPG 2.95

Table 15

Non-Isothermal Hot-Wire RMS Voltage Fluctuation Data for r/R=.5

$\Delta P(in)$* → $R_w - \bar{R}_a$ (Ohm) ↓	2.120		1.620	1.330	0.932	0.480
1.00	42.9	Milli-volts	45.0	46.8	50.5	59.7
1.20	42.9		44.8	46.8	50.0	58.3
1.40	42.6		44.6	46.2	49.2	57.1
1.60	42.6		44.0	45.8	48.7	56.2
1.80	42.7		44.0	45.6	48.0	55.0
2.00	42.7		43.8	45.1	47.5	54.2
2.20	42.3		43.5	44.9	47.0	52.8
2.40	42.3		43.3	44.8	46.2	52.2
2.60	42.2		43.2	44.5	46.0	51.7
2.80	42.8		43.2	44.5	45.8	50.8
3.00	42.6		43.0	44.3	45.2	50.3
3.20	42.6		43.0	44.3	45.1	49.5
3.40	42.6		43.0	44.0	44.8	49.2

* Orifice Meter Manometer Fluid SPG 2.95

Table 16

Non-Isothermal Hot-Wire "After" Calibration Data

ΔP (in)* → $R_w-\bar{R}_a$ (Ohm) ↓	2.120	1.620	1.330	0.932	0.480
1.00	2.010 (Volts)	1.945	1.920	1.860	1.775
1.20	2.140	2.100	2.070	1.985	1.890
1.40	2.235	2.215	2.180	2.120	2.000
1.60	2.365	2.320	2.285	2.220	2.125
1.80	2.470	2.420	2.385	2.320	2.215
2.00	2.565	2.515	2.480	2.405	2.295
2.20	2.655	2.600	2.565	2.495	2.375
2.40	2.740	2.685	2.645	2.570	2.450
2.60	2.820	2.765	2.720	2.645	2.525
2.80	2.900	2.840	2.795	2.720	2.595
3.00	2.970	2.915	2.860	2.785	2.655
3.20	3.070	2.980	2.930	2.845	2.715
3.40	3.135	3.075	2.995	2.910	2.775

* Orifice Meter Manometer Fluid SPG 2.95

Table 17

Cold Resistances in"After"Calibration

P (in.)*	R_{cold} (OHM)
2.120	7.21
1.620	7.24
1.330	7.26
0.932	7.29
0.480	7.43

APPENDIX B

APPENDIX B

ORIFICE METER CALIBRATION

The orifice meter used was calibrated in place against a pitot tube located at the centerline of the test section. von Karman's universal velocity distribution[18] was used to calculate flow rates from the pitot tube velocity measurements. The calibration curve is shown in Figure 14. It is found as anticipated that a plot of flow rate versus the square root of the pressure drop is a straight line.[19]

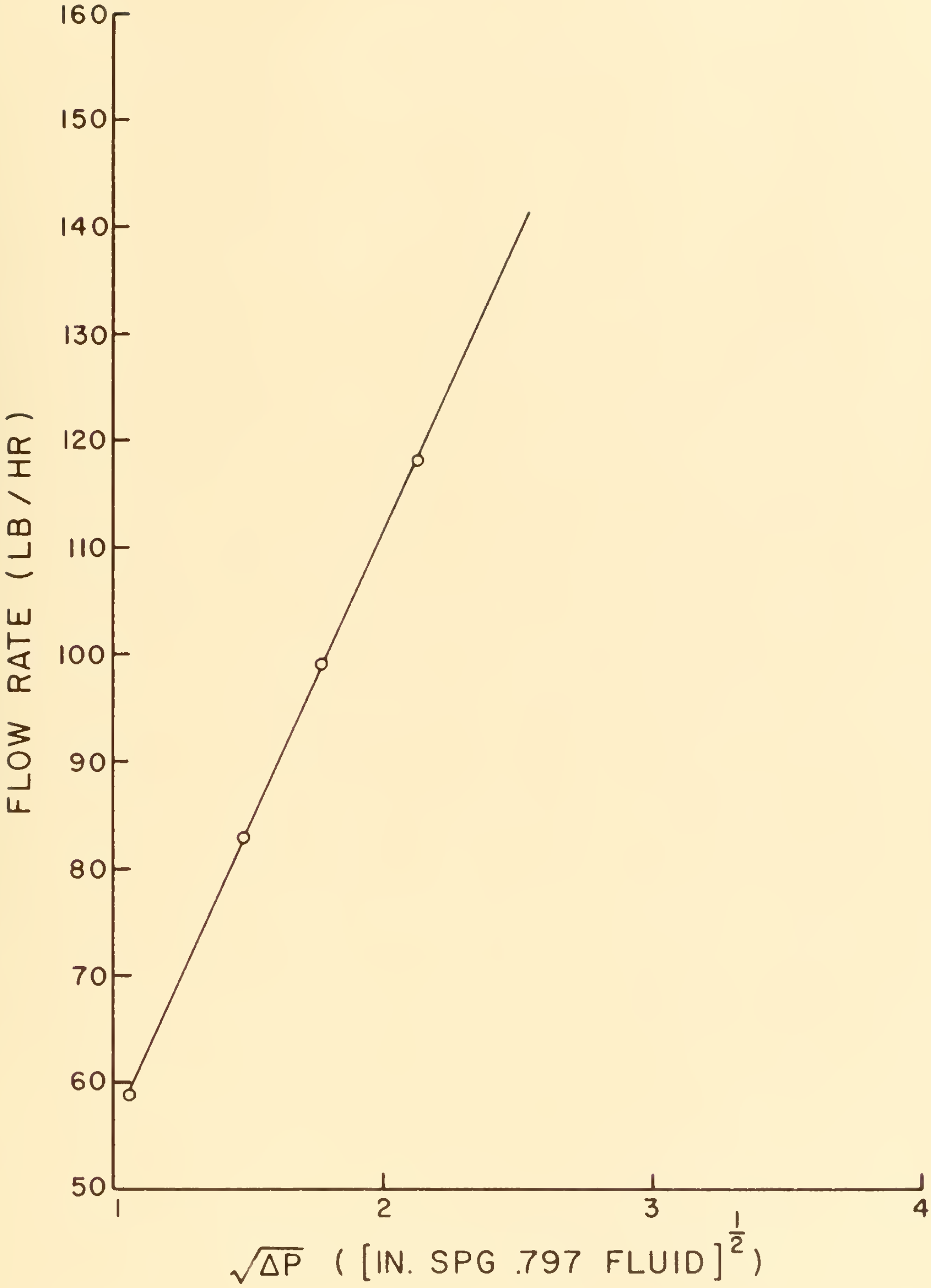

Figure 14. Orifice Meter Calibration Curve

APPENDIX C

APPENDIX C

AMPLIFIER FREQUENCY RESPONSE

The frequency response of the Tektronix amplifier is shown on the following page.

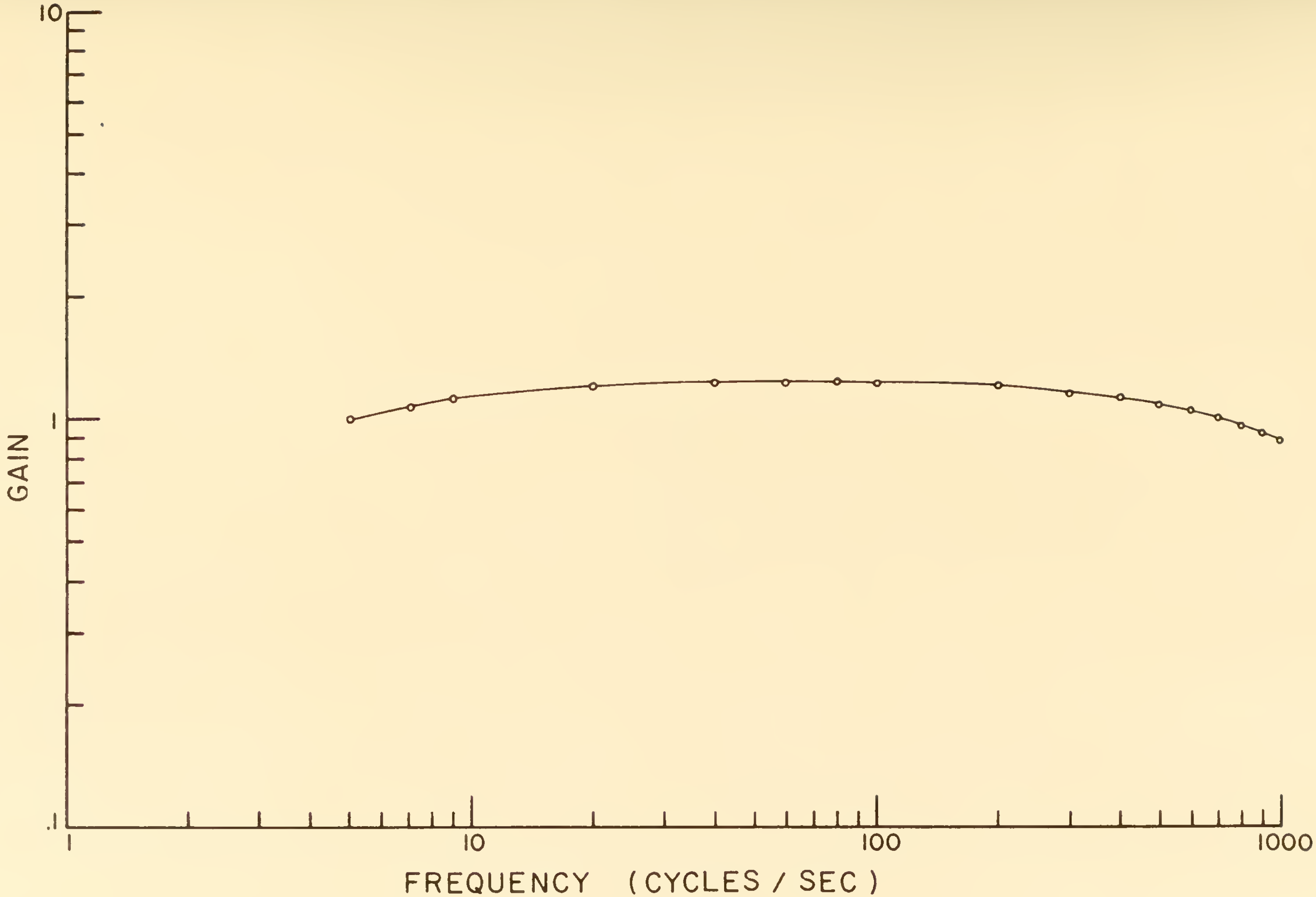

Figure 15. Amplifier Frequency Response

APPENDIX D

APPENDIX D

RESISTANCE-TEMPERATURE CURVE FOR THE HOT-WIRE

Figure 16 shows the relationship between resistance and temperature for the hot wire used in the non-isothermal flow measurements. The dashed curve is the approximate relationship suggested by Kronauer.[3]

Figure 16. Resistance-Temperature Curve for Hot-Wire

APPENDIX E

APPENDIX E

CALIBRATION OF HOT-WIRE IN ISOTHERMAL FLOW

The isothermal flow data were taken on two different days. The set of data for a Reynolds Number of 49,800 was taken on the first day. The calibration curve for these data is shown in Figure 17. The constant C in Equation 18, which is the slope of the line in Figure 17 is 1.67×10^{-2}.

The data at Reynolds Numbers of 30,700 and 41,500 were taken on the second day. The calibration curve for these data is shown in Figure 18. The constant C for these data is 1.69×10^{-2}.

The value of C calculated from Equation 17 is 0.84×10^{-2}. The discrepancy between this value and that obtained from calibration is due to wire history effects in α and R_o and the error inherent in King's potential flow value for B.

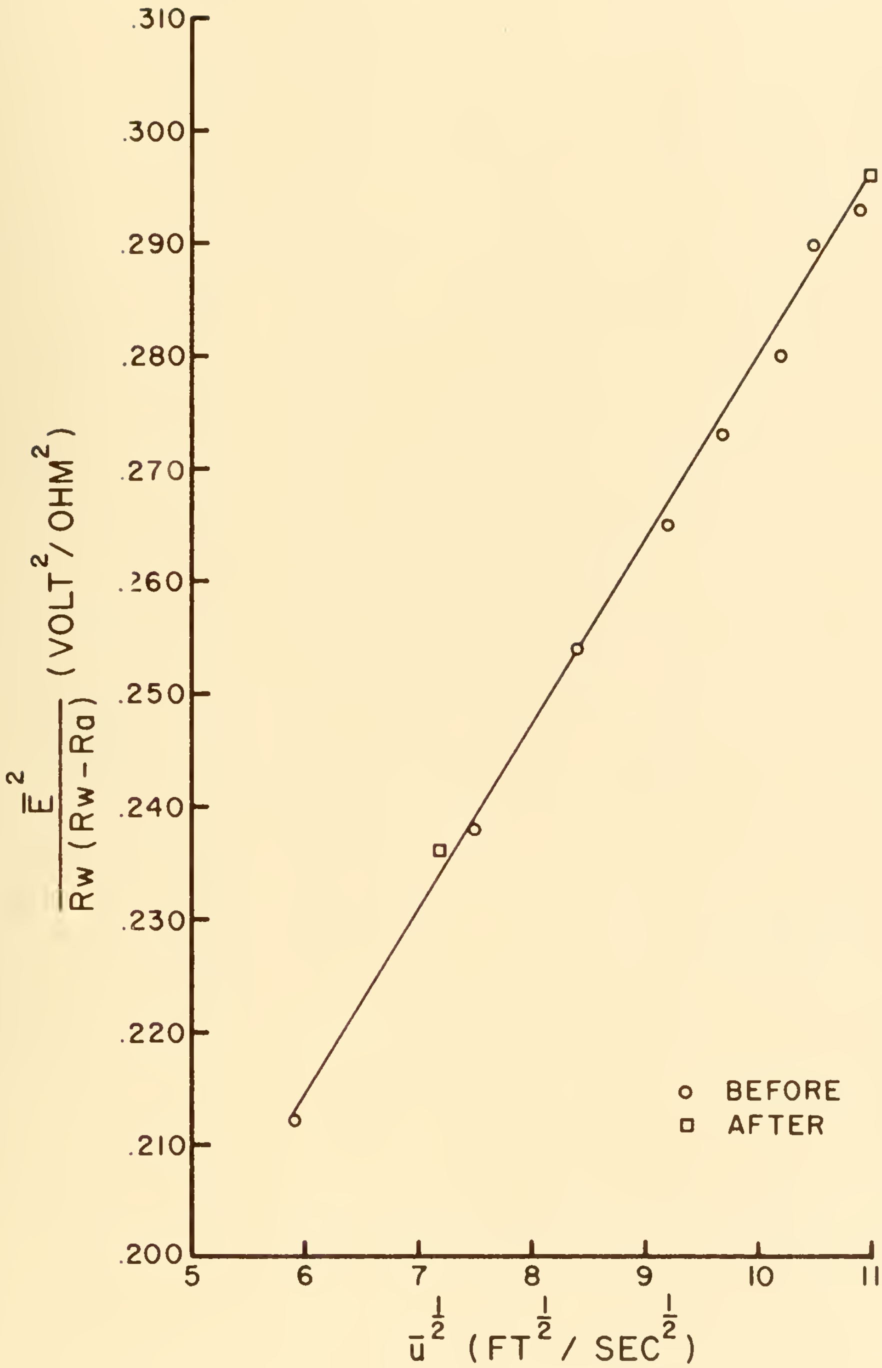

Figure 17. Isothermal Calibration of Hot-Wire I

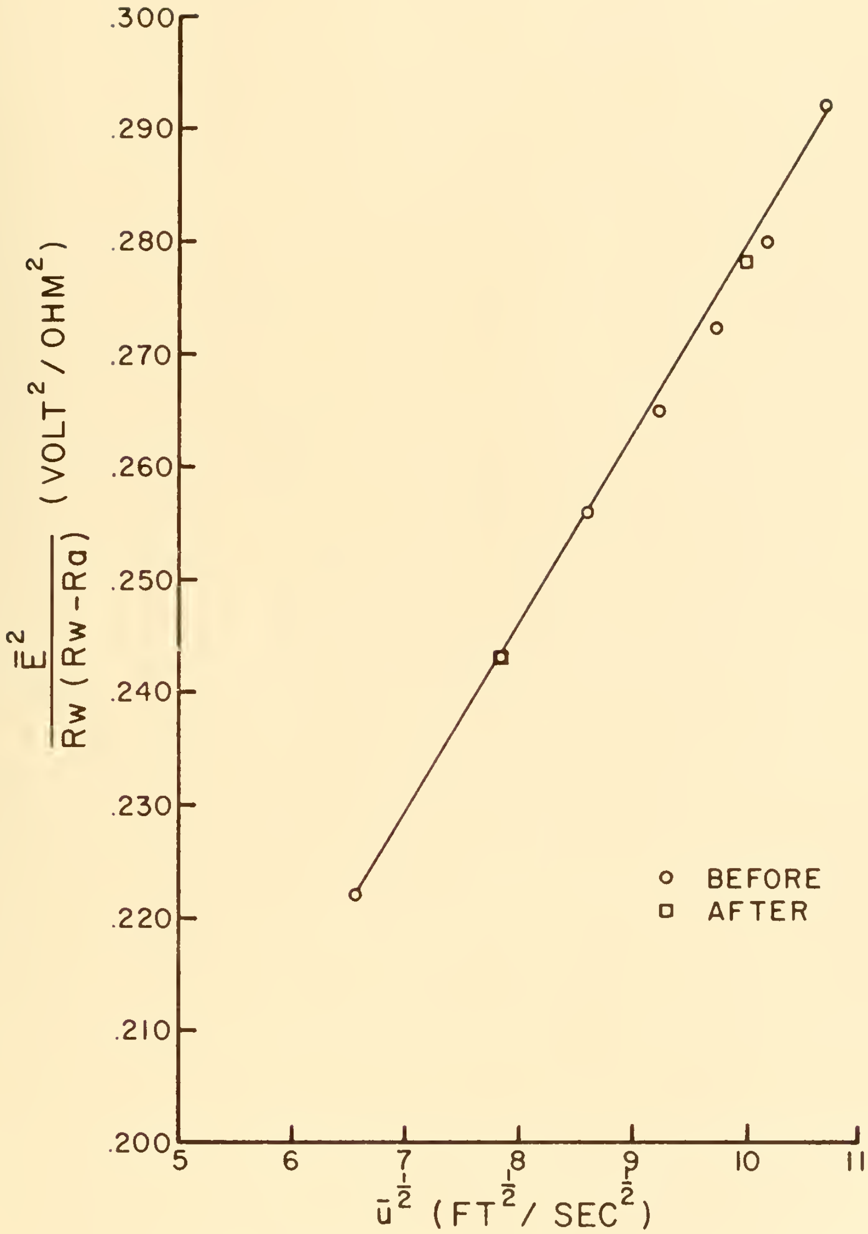

Figure 18. Isothermal Calibration of Hot-Wire II

APPENDIX F

APPENDIX F

LISTING OF CURVE FITTING PROGRAM

The computer subroutine used to perform least square curve fitting calculations is listed on the following pages.

```
                 SUBROUTINE POLYFT (X, Y, N, KOR, C, CO, A, NOUT)
           C
           C     DIMENSION  FOR ARGUMENTS
000011           DIMENSION  X(15),Y(15),A(225),C(15)
           C
           C     DIMENSION  FOR SELF-GENERATED VALUES
000011           DIMENSION  SUMX(50),SMYX(50),AMEANX(50)
000011           MIS= 0
000012           KTOR= 2*KOR
           C
           C     INITIALIZATION
000014           DO  1   I=1,KOR
000015           SMYX(I)= 0.0
000017         1 AMEANX(I)= 0.0
000022           DO  2   I=1,KTOR
000023         2 SUMX(I)= 0.0
000027           SUMY= 0.0
           C
           C     NORMALIZATION WITH RESPECT TO AMAX
000027           XMAX= X(1)
000031           DO  100  I=2,N
000033           IF ( X(I) -XMAX) 100,101,101
000036       101 XMAX= X(I)
000041       100 CONTINUE
000044           DO  102  I=1,N
000045       102 X(I)= X(I)/XMAX
           C
           C
           C     FORMULATION OF NORMAL EQUATIONS
000051           DO  3  J=1,KTOR
  0053           DO  3  I=1,N
000054         3 SUMX(J)= SUMX(J) +X(I)**J
000067           DO  4  I=1,N
```

```
000071          4 SUMY= SUMY+ Y(I)                                      POLY0360
000075            AMEANY=SUMY/PTS
000077            DO 6 J=1,KOR
000100            AMEANX(J)= SUMX (J)/PTS                               POLY0370
000104            DO 6 I=1,N                                            POLY0380
000105          6 SMYX(J)= SMYX(J) +Y(I)*X(I)**J                        POLY0390
000122            DO 8 I=1,KOR                                          POLY0400
000123            C(I)= SMYX(I) -PTS*AMEANX(I)*AMEANY                   POLY0410
000132            DO 8 J=1,KOR                                          POLY0420
000133            K= I+J                                                POLY0430
000134            IJ =(J-1)*KOR +I                                      POLY0440
000137          8 A(IJ) =SUMX(K) -PTS* AMEANX(I)*AMEANX(J)              POLY0450
        C                                                               POLY0460
        C         CROUTS REDUCTION METHOD                               POLY0470
000155            DO 11 I=2,KOR                                         POLY0480
000156            II1=(I-1)*KOR + 1                                     POLY0490
000161         11 A(II1) = A(II1)/ A(1)                                 POLY0500
000167            DO 12 J=2,KOR                                         POLY0510
000170            KM= J-1                                               POLY0520
000172            DO 14 I= J,KOR                                        POLY0530
000173            AP1= 0.0                                              POLY0540
000174            DO114 K=1,KM                                          POLY0550
000176            IK =(K-1)* KOR+ I                                     POLY0560
000201            KJ =(J-1)* KOR+ K                                     POLY0570
000204        114 AP1 = AP1 + A(IK) *A(KJ)                              POLY0580
000215            IJ =(J-1)* KOR+ I                                     POLY0590
000220         14 A(IJ) = A(IJ) -AP1                                    POLY0600
000226            JP= J+1                                               POLY0610
000227            IF (JP- KOR) 444, 444, 445                            POLY0620
000232        444 DO 16 I= JP,KOR                                       POLY0630
000234            AP1= 0.0                                              POLY0640
000235            DO116 K=1,KM                                          POLY0650
000237            JK =(K-1)* KOR + J                                    POLY0660
000242            KI =(I-1)* KOR + K                                    POLY0670
000245        116 AP1 =AP1 +A(JK) *A(KI)                                POLY0680
000256            JI =(I-1)* KOR + J                                    POLY0690
000261            JJ =(J-1)* KOR + J                                    POLY0700
000264         16 A(JI) = (A(JI) -AP1)/A(JJ)                            POLY0710
000274        445 DUMMY= 0.0                                            POLY0720
000275         12 CONTINUE                                              POLY0730
000300            C(1) =C(1)/A(1)                                       POLY0740
000302            DO 18 I=2,KOR                                         POLY0750
000304            AP1= 0.0                                              POLY0760
000305            IM=I-1                                                POLY0770
000307            DO 118 K=1,IM                                         POLY0780
000310            IK =(K-1)* KOR + I                                    POLY0790
000313        118 AP1=AP1 +A(IK) *C(K)                                  POLY0800
000324            II =(I-1)* KOR + I                                    POLY0810
000327         18 C(I) =(C(I)- AP1) / A(II)                             POLY0820
000336            KORM= KOR-1                                           POLY0830
000337            IF (KORM) 122, 123,122                                POLY0840
000340        122 DO 21 I=1,KORM                                        POLY0850
000342            AP1= 0.0                                              POLY0860
000343            M= KOR-I                                              POLY0870
000344            MP= M+1                                               POLY0880
000346            DO 121 K=MP,KOR                                       POLY0890
000347            MK =(K-1)* KOR +M                                     POLY0900
000352        121 AP1 =AP1 + A(MK)* C(K)                                POLY0910
000362         21 C(M) =C(M) -AP1                                       POLY0920
000367        123 AP1= 0.0                                              POLY0930
```

```
000370         DO 24   I=1,KOR                                                            POLY0940
000372      24 API =API +AMEANX(I) *C(I)                                                  POLY0950
000400         CO  = AMEANY -API                                                          POLY0960
       C                                                                                  POLY0970
       C       RENORMALIZATION WITH RESPECT TO XMAX                                       POLY0990
000401     777 DO 779 I = 1,KOR                                                           POLY1000
000403     779 C(I) = C(I)/XMAX**I                                                        POLY1010
       C                                                                                  POLY1130
000413         DO 35 I=1,N
000414      35 X(I)=X(I)*XMAX
000420     778 SRES=0.0
000421         DO 877 I=1,N
000423         SMOOTH=CO
000424         DO 27 J=1,KOR
000426      27 SMOOTH=SMOOTH+C(J)*X(I)**J
000440         RES=Y(I)-SMOOTH
000442         SRES=SRES+RES**2
000444     877 CONTINUE
000447         STDV=SQRT(SRES/PTS)
000452         IF(NCUT.EQ.0) RETURN
000455      36 WRITE(6,29)
000461      29 FORMAT      (60H                X                 Y              SMOOTH    POLY1050
              1      RES             )                                                    POLY1060
000461         DO 77 I=1,N
000466         SMOOTH=CO
000467         DO 37 J=1,KOR
000471      37 SMOOTH=SMOOTH+C(J)*X(I)**J
000503         RES=Y(I)-SMOOTH
000506      30 FORMAT( 4F15.4)                                                            POLY1160
000506      77 WRITE(6,30) X(I),Y(I),SMOOTH,RES
000537         WRITE(6,31) STDV
000544      31 FORMAT      (10H0STDV     =F20.5)                                          POLY1200
000544         WRITE(6,33) CO
000556      33 FORMAT(10H0CO        =E20.10)
000556         WRITE(6,32) (C(I), I=1,KOR)
000601      32 FORMAT(10H0C(I)      /(5F20.10/))
000601         RETURN                                                                     POLY1270
000602         END                                                                        POLY1280

UNUSED COMPILER SPACE
001200
```

APPENDIX G

APPENDIX G

CALIBRATION OF HOT-WIRE IN NON-ISOTHERMAL FLOW

Figures 19 through 23 represent the calibration data used to compute the results presented for non-isothermal flow. The curves drawn through the data represent the least squares fit of parabolas to the data. These parabolas were differentiated analytically to obtain the values of S_u and S_T presented in Figures 9 and 10.

Figures 24 through 26 show calibration curves for representative values of $\bar{u}$ and $T_w - \bar{T}_a$ before and after fluctuation measurements were made. Table 18 gives a complete tabulation of S_u and S_T as functions of $\bar{u}$ and $T_w - \bar{T}_a$ before and after the fluctuation measurements.

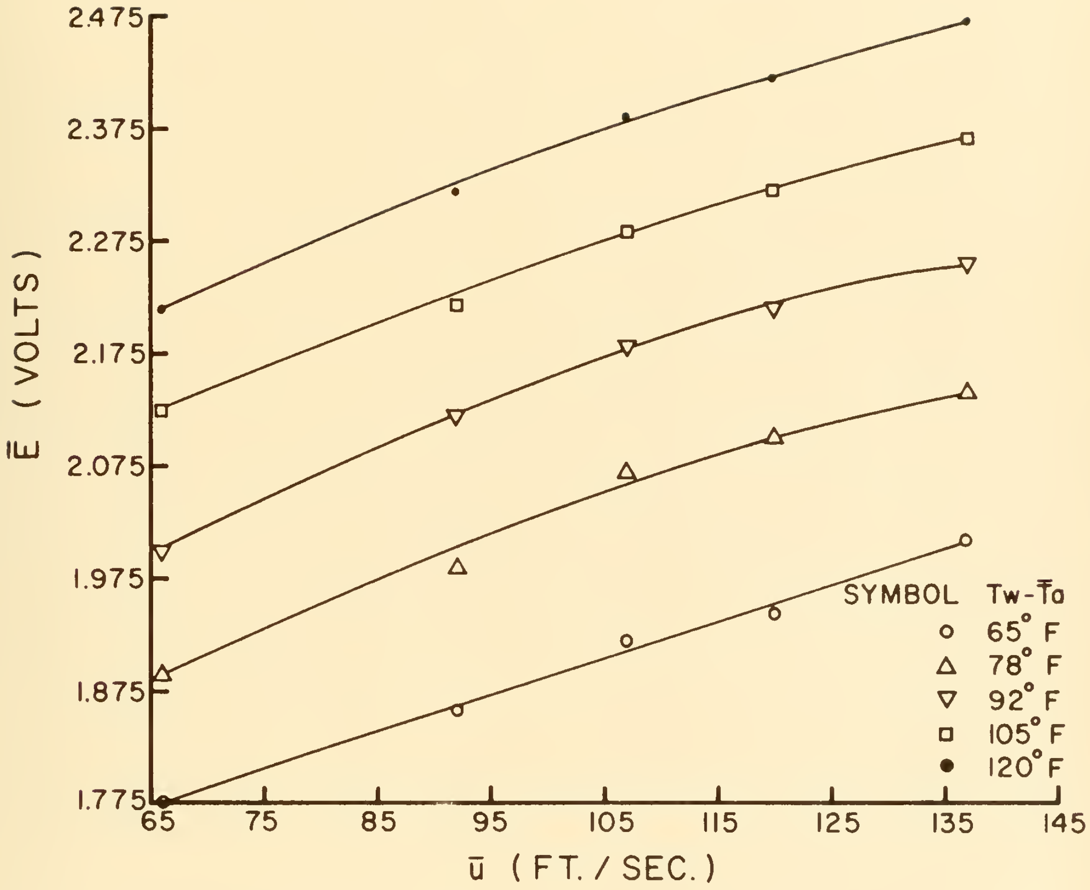

Figure 19. Non-Isothermal Calibration of Hot-Wire I

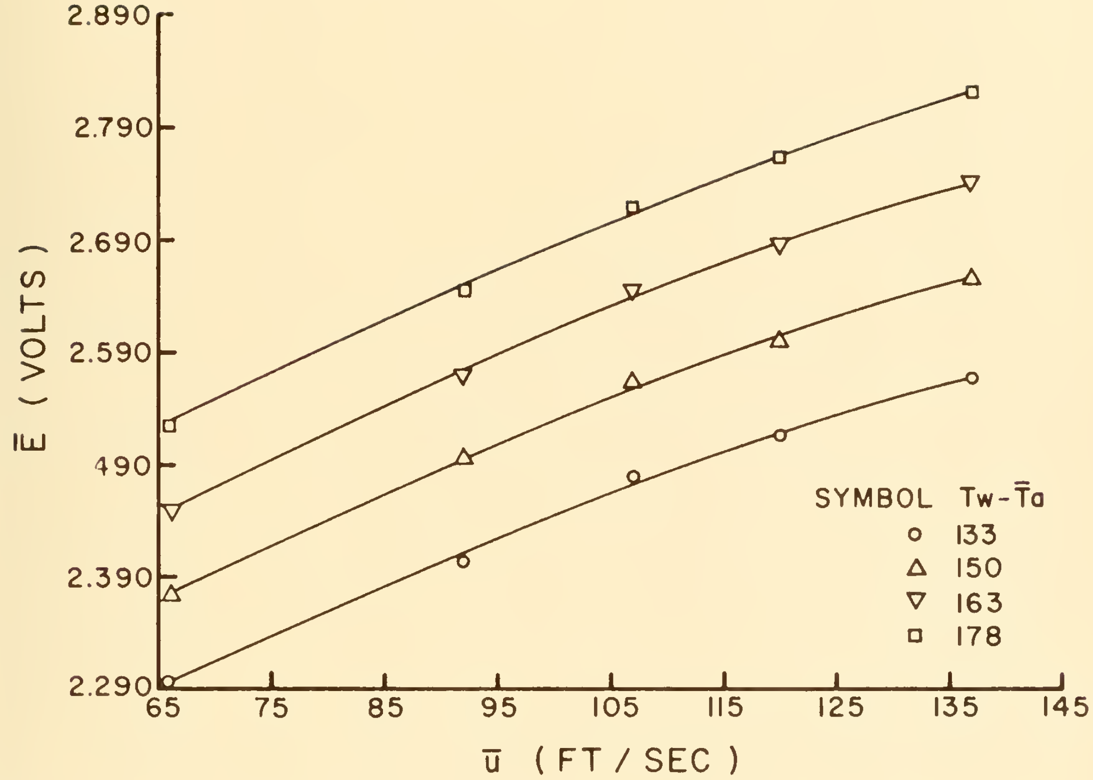

Figure 20. Non-Isothermal Calibration of Hot-Wire II

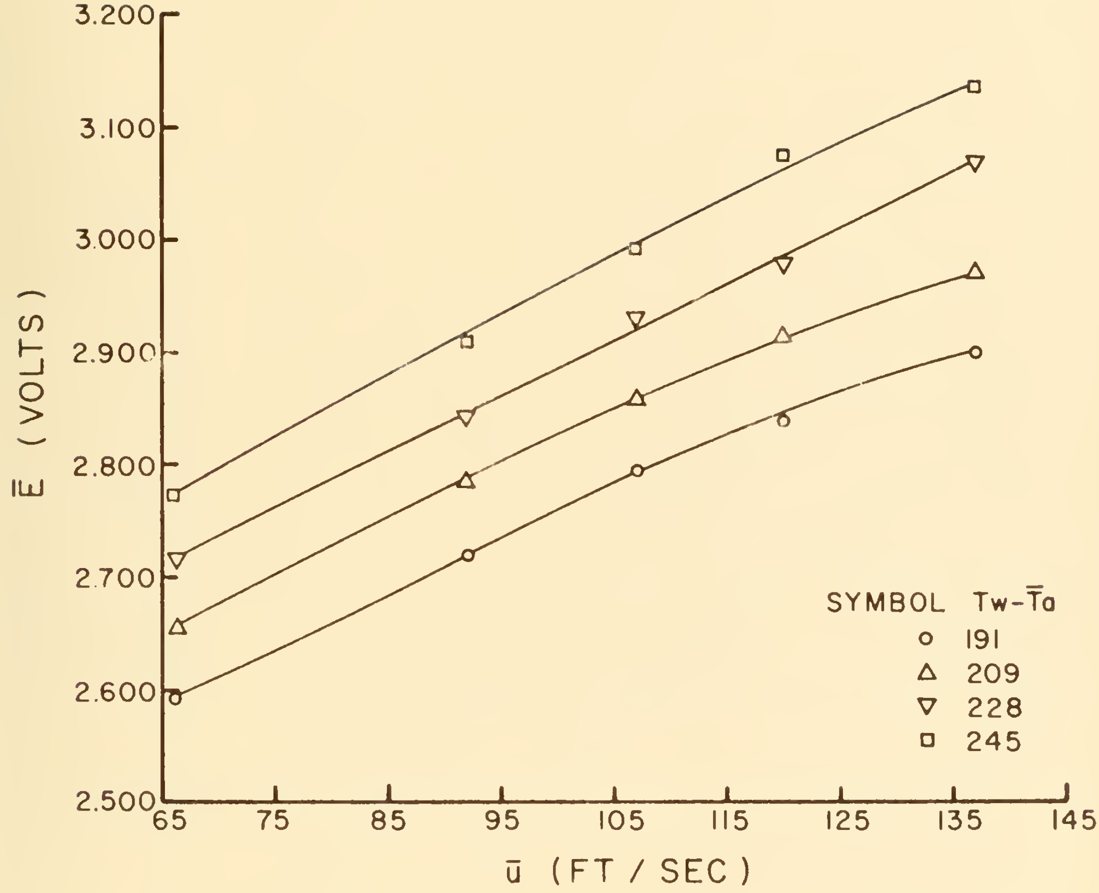

Figure 21. Non-Isothermal Calibration of Hot-Wire III

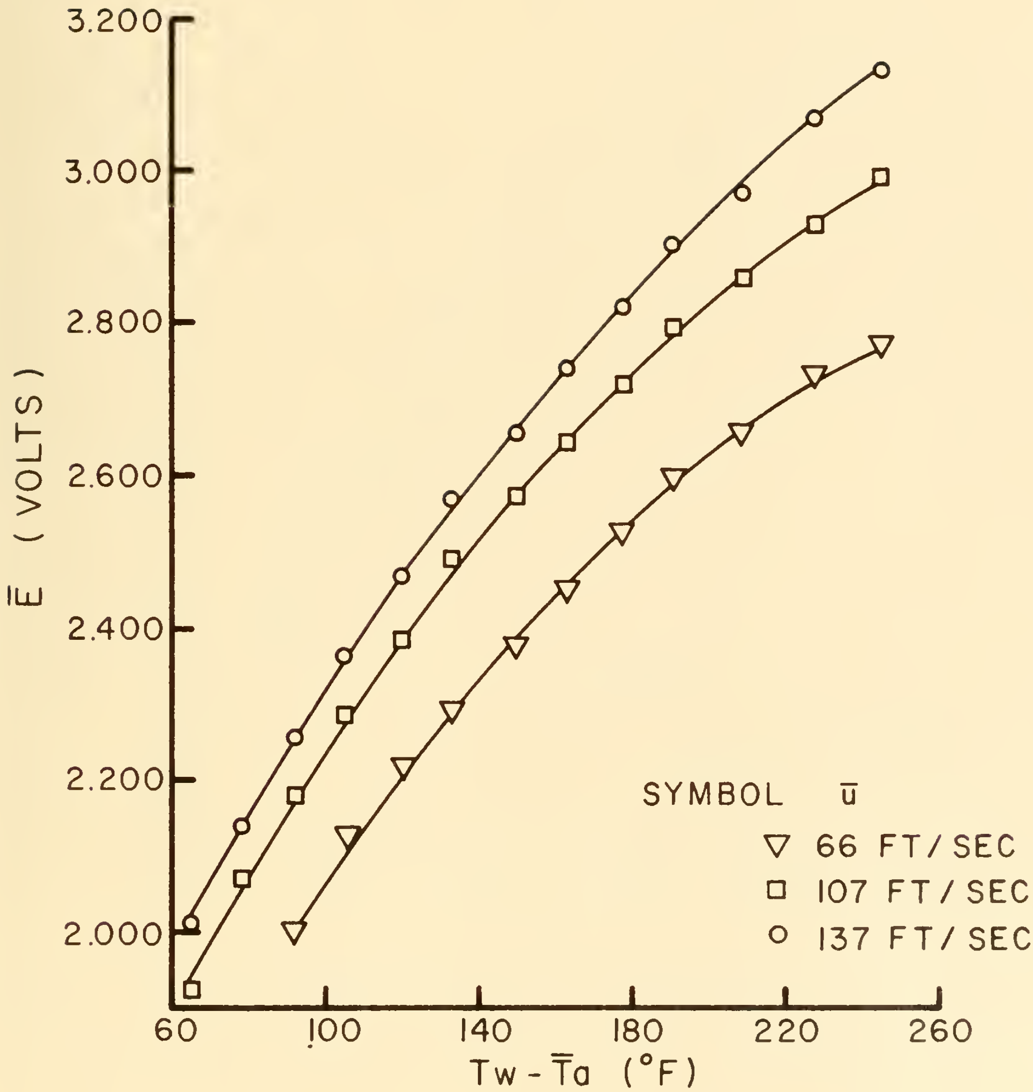

Figure 22. Non-Isothermal Calibration of Hot-Wire IV

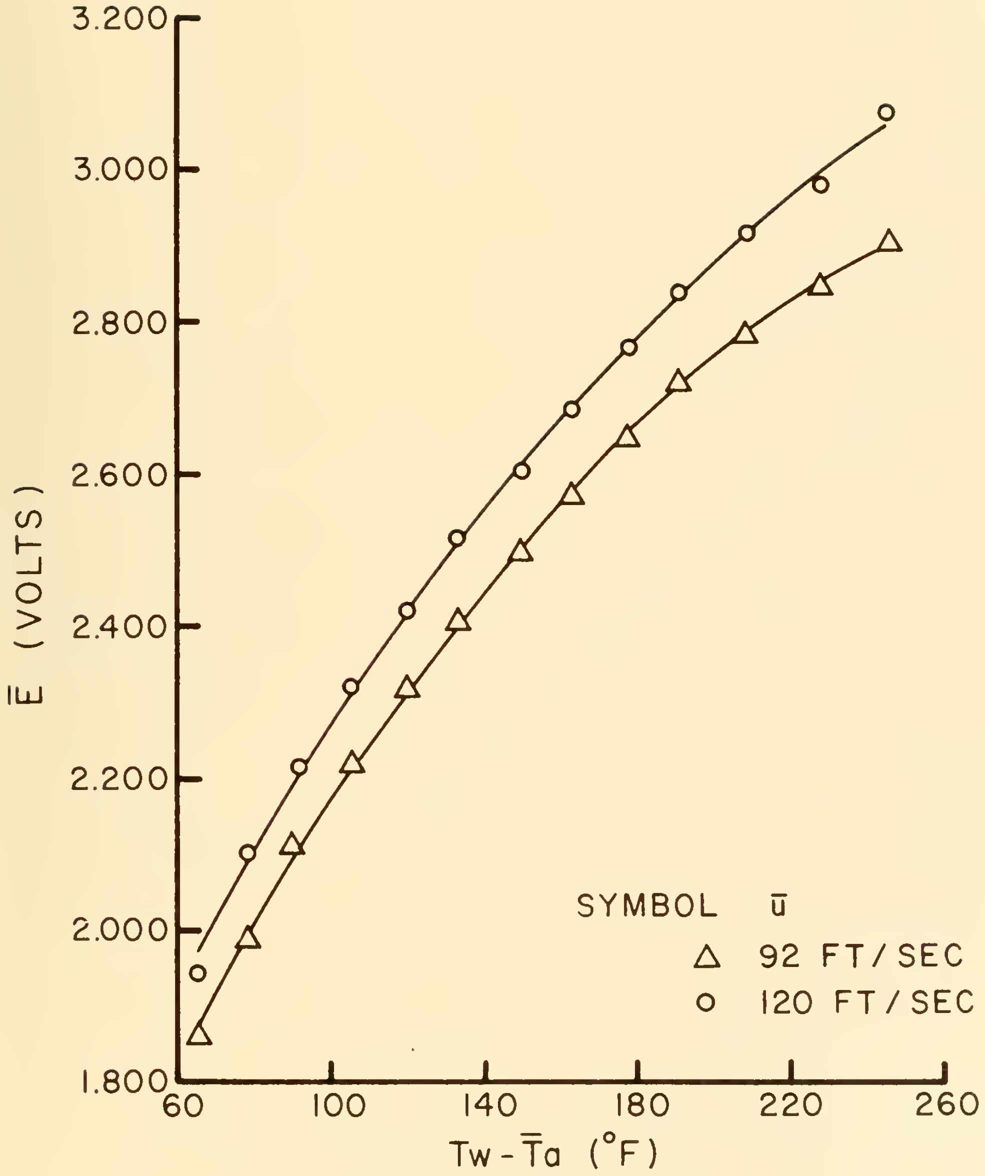

Figure 23. Non-Isothermal Calibration of Hot-Wire V

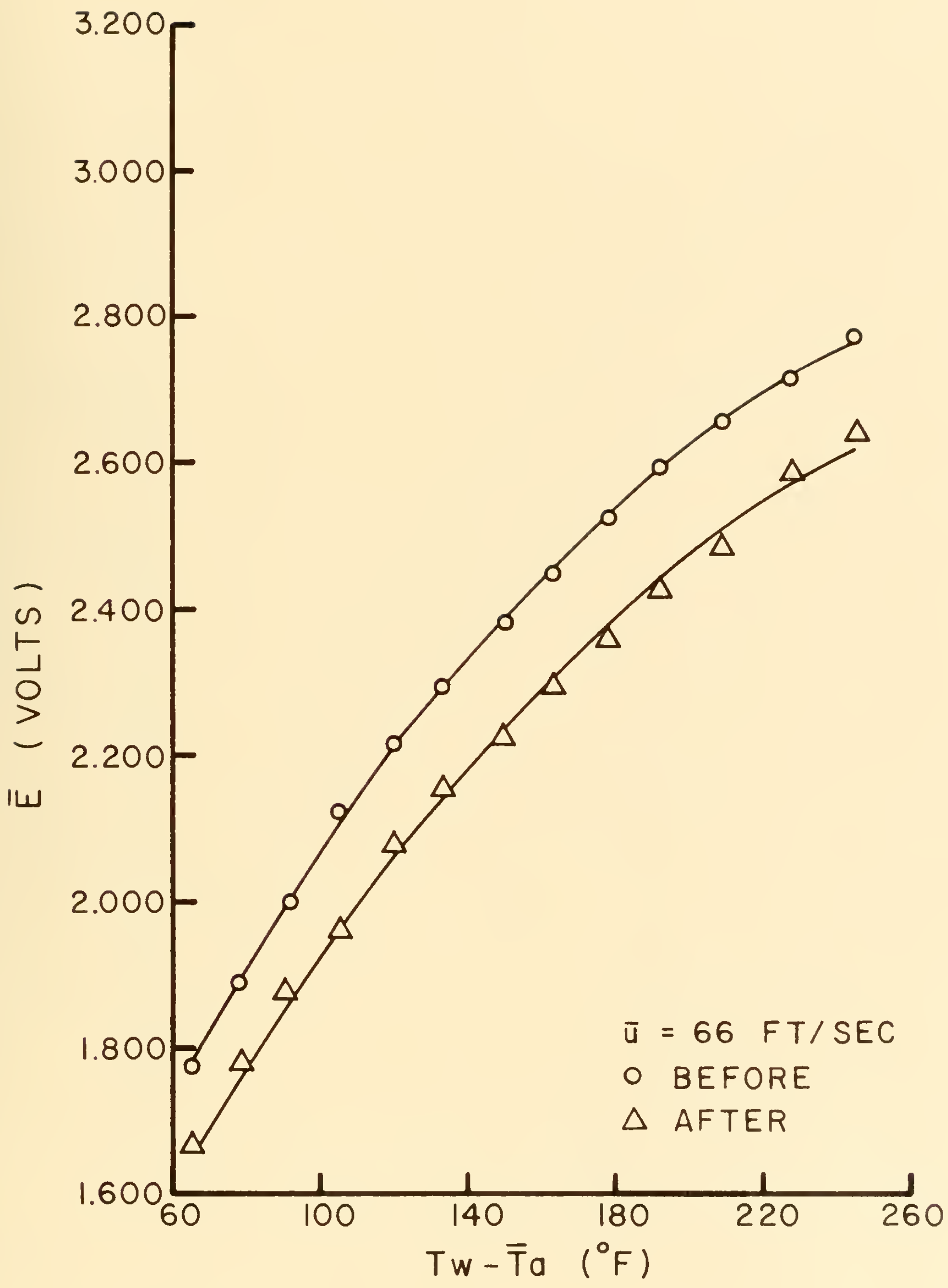

Figure 24. Calibration Drift I

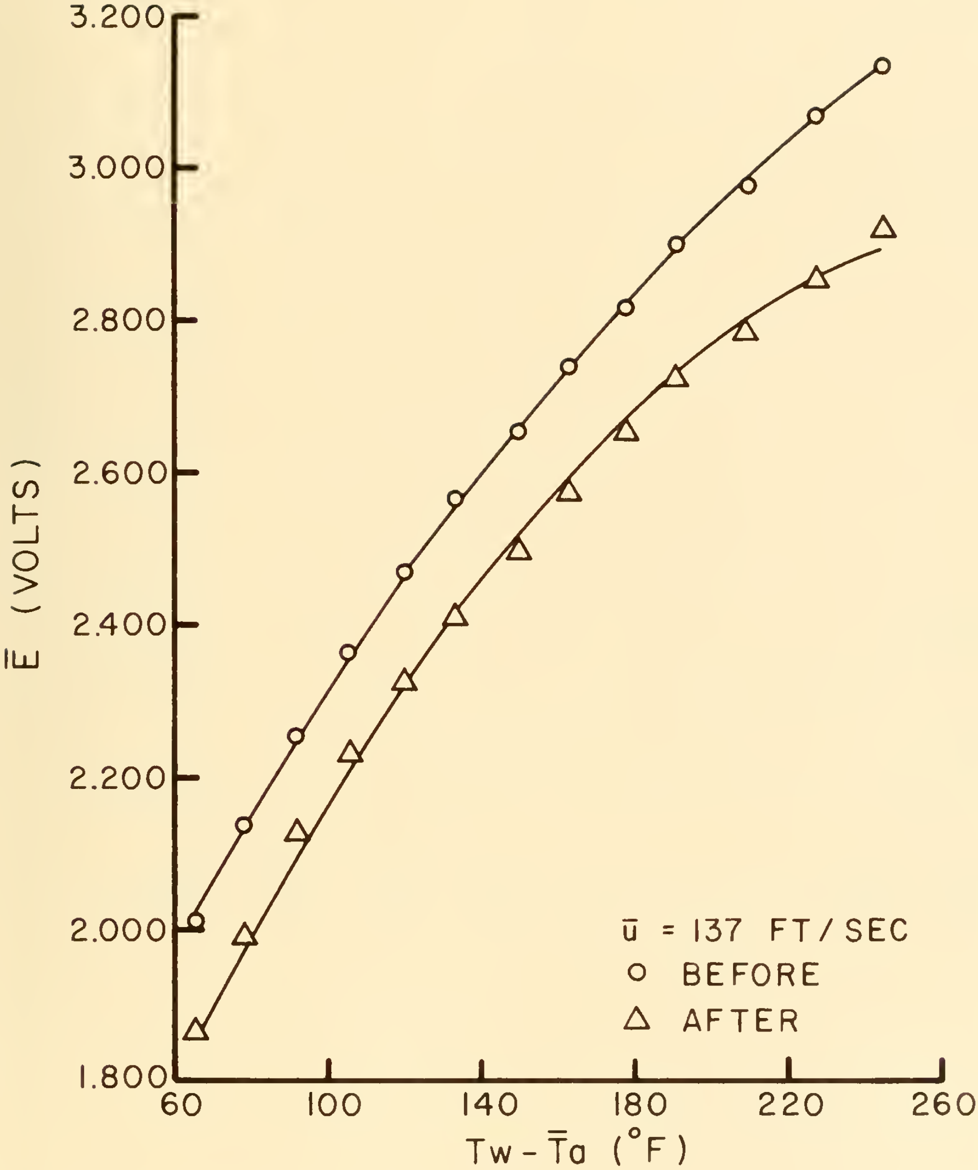

Figure 25. Calibration Drift II

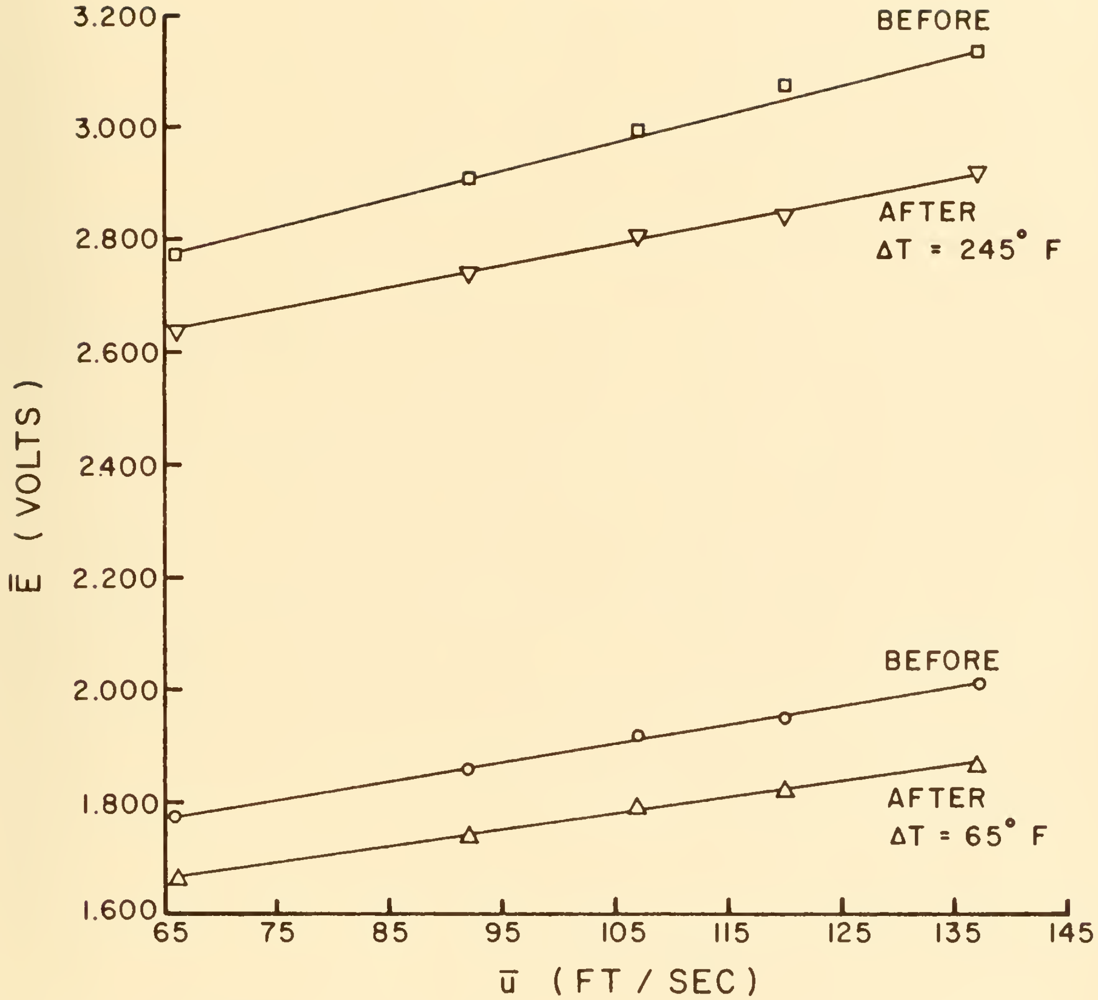

Figure 26. Calibration Drift III

Table 18

Values of S_u and S_T for Successive Calibrations

$\bar{u}$ (Ft/Sec)

$T_w-\bar{T}_a$	66		92		107		120		137	
^oF	S_u	S_T	S_u	S_T	S_u	S_T	S_u	S_T	S_u	S_T
65	3.39	8.5	3.31	8.9	3.25	8.9	3.21	8.9	3.15	8.8
	3.48	8.2	3.16	9.1	2.97	9.3	2.82	9.5	2.61	9.7
78	4.87	8.1	3.96	8.5	3.44	8.5	2.98	8.5	2.39	8.4
	3.61	7.8	3.38	8.6	3.25	8.8	3.15	8.9	3.03	9.2
92	5.34	7.6	4.07	8.0	3.33	8.0	2.68	8.1	1.85	8.0
	4.29	7.4	4.00	8.0	3.82	8.2	3.68	8.3	3.48	8.6
105	4.30	7.1	3.66	7.5	3.29	7.5	2.97	7.6	2.55	7.6
	5.46	6.9	4.42	7.4	3.78	7.6	3.30	7.7	2.61	7.9
120	4.61	6.6	3.88	7.0	3.45	7.0	3.08	7.1	2.60	7.2
	4.45	6.5	3.93	6.9	3.60	7.0	3.36	7.1	3.02	7.3
133	5.70	6.2	5.08	6.5	4.72	6.6	4.41	6.7	4.01	6.8
	4.99	6.1	4.20	6.4	3.70	6.5	3.34	6.6	2.80	6.7
150	5.25	5.6	4.29	5.9	3.74	6.0	3.27	6.2	2.64	6.3
	4.87	5.5	4.32	5.8	3.97	5.8	3.71	5.9	3.34	6.0
163	5.33	5.1	4.44	5.4	3.92	5.5	3.47	5.8	2.89	5.9
	5.09	5.1	4.47	5.2	4.08	5.2	3.80	5.3	3.39	5.4
178	5.31	4.6	4.49	4.9	4.02	5.0	3.61	5.3	3.08	5.5
	5.63	4.6	4.70	4.7	4.11	4.6	3.67	4.7	3.05	4.8

Table 16 (cont'd.)

191	5.41	4.1	4.61	4.4	4.14	4.5	3.74	4.9	3.21	5.1
	5.64	4.2	4.81	4.1	4.29	4.0	3.91	4.0	3.36	4.1
209	5.68	3.5	4.81	3.7	4.30	3.9	3.86	4.3	3.29	4.5
	5.72	3.7	4.88	3.5	4.35	3.4	3.96	3.4	3.40	3.4
228	5.18	2.8	5.03	3.0	4.94	3.2	4.87	3.7	4.77	4.0
	3.96	3.1	4.05	2.8	4.11	2.7	4.15	2.7	4.21	2.7
245	5.88	2.3	5.38	2.4	5.08	2.7	4.83	3.1	4.50	3.5
	4.07	2.6	4.18	2.2	4.24	2.0	4.29	2.0	4.37	2.0

Before
After

APPENDIX H

APPENDIX H

KOVASZNAY FLUCTUATION DIAGRAMS

Figures 27 through 29 show the Kovasznay Fluctuation Diagrams for three representative cases.

The parabolas that fit these data are:

Figure	Parabola
27	$\left(\frac{\overline{e'^2}}{S_T^2} - \overline{t'^2}\right) = 2.64 + 16.9\left(\frac{S_u}{S_T}\right) + 19.1\left(\frac{S_u}{S_T}\right)^2$
28	$\left(\frac{\overline{e'^2}}{S_T^2} - \overline{t'^2}\right) = 0.43 + 18.9\left(\frac{S_u}{S_T}\right) + 16.2\left(\frac{S_u}{S_T}\right)^2$
29	$\left(\frac{\overline{e'^2}}{S_T^2} - t'^2\right) = 0.21 + 42.6\left(\frac{S_u}{S_T}\right) + 47.3\left(\frac{S_u}{S_T}\right)^2$.

$\overline{u't'}$ is then found by dividing the coefficient of $\frac{S_u}{S_T}$ by -2, and $\sqrt{\overline{u'^2}}$ is the square root of the coefficient of $\left(\frac{S_u}{S_T}\right)^2$. The results from the parabolas given above are listed in Table 19.

Table 19

Sample Results for $\sqrt{\overline{u'^2}}$ and $\overline{u't'}$

Reynolds Number	And r/R	$\sqrt{\overline{u'^2}}$	$\overline{u't'}$
27,400	0.0	4.36	-8.45
38,200	0.0	4.03	-9.45
38,200	0.5	6.89	-21.3

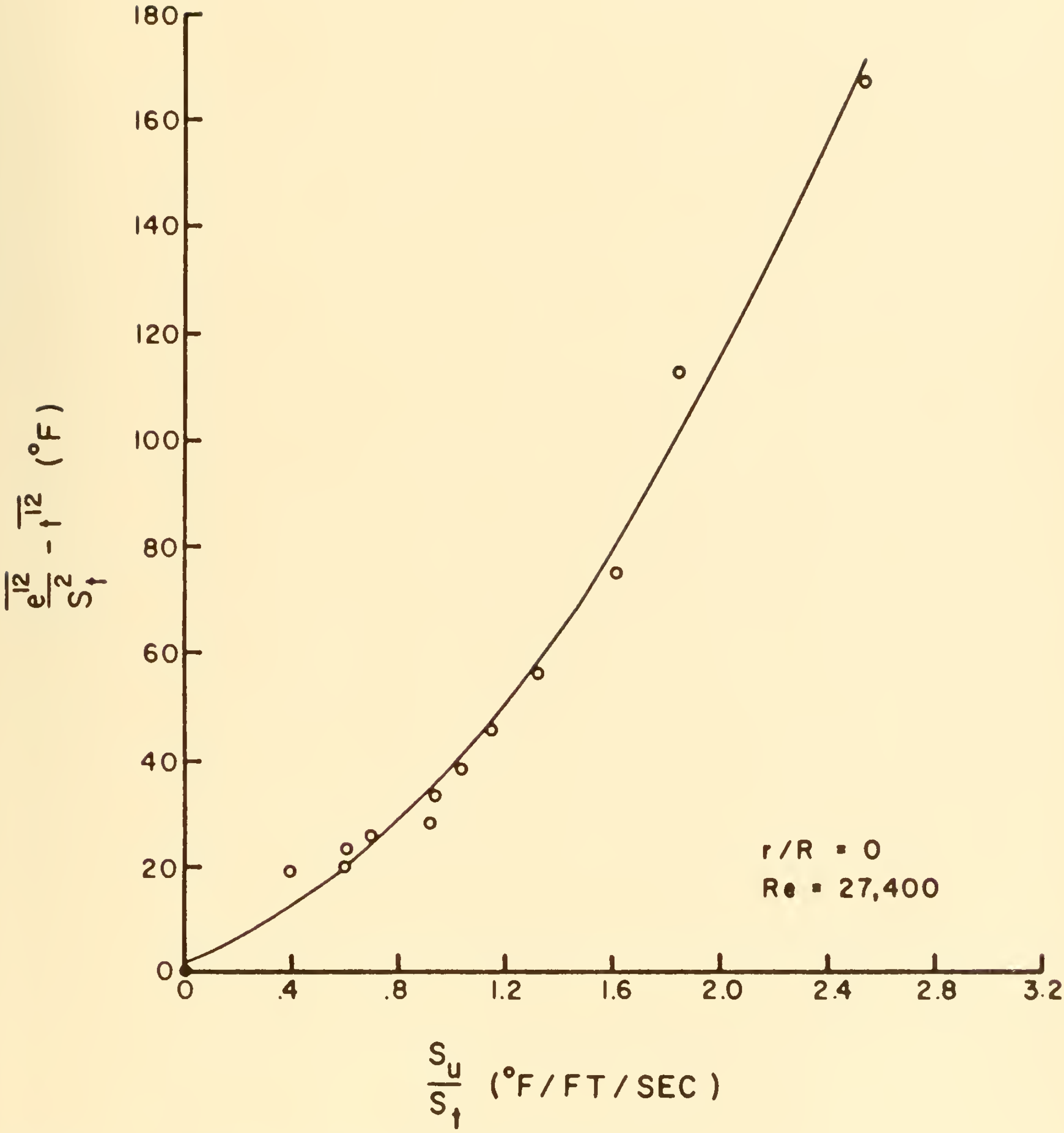

Figure 27. Kovasznay Fluctuation Diagram I

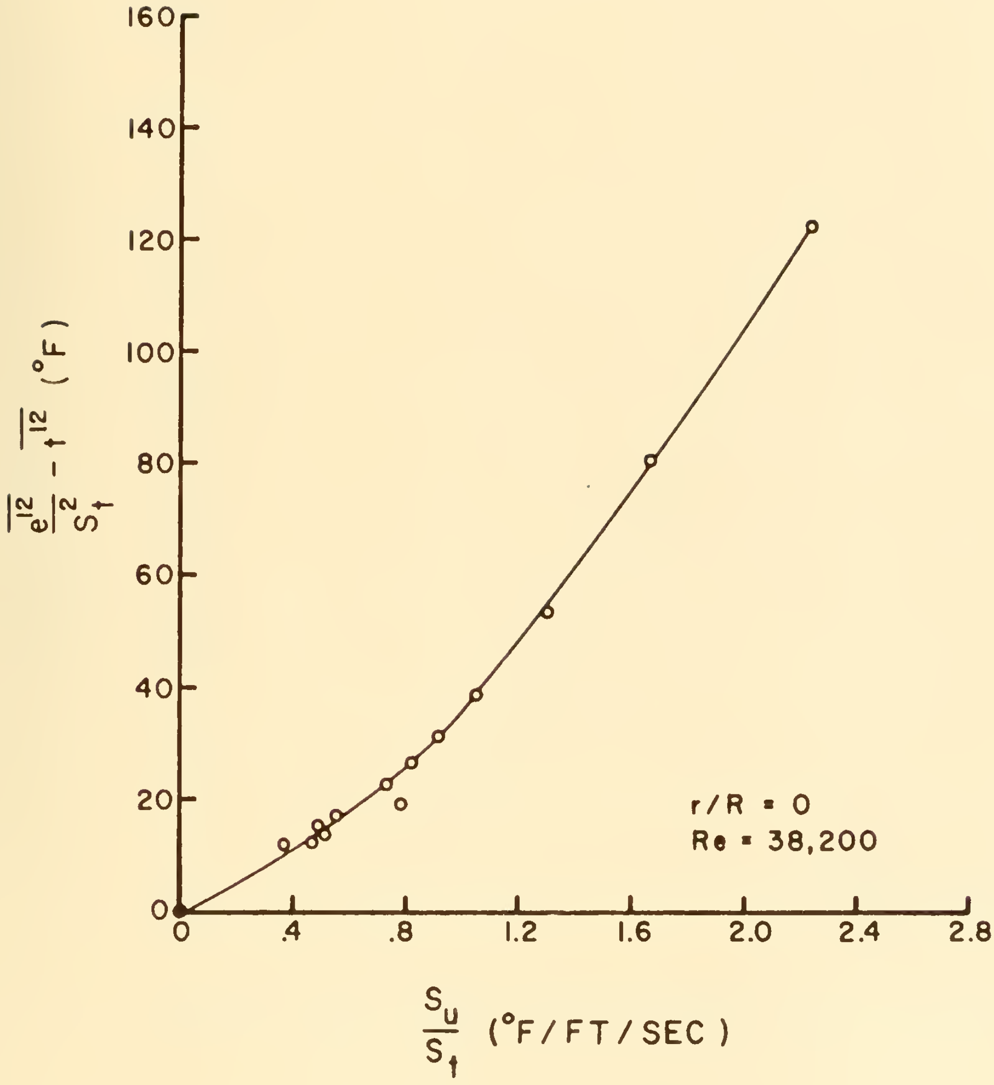

Figure 28. Kovasznay Fluctuation Diagram II

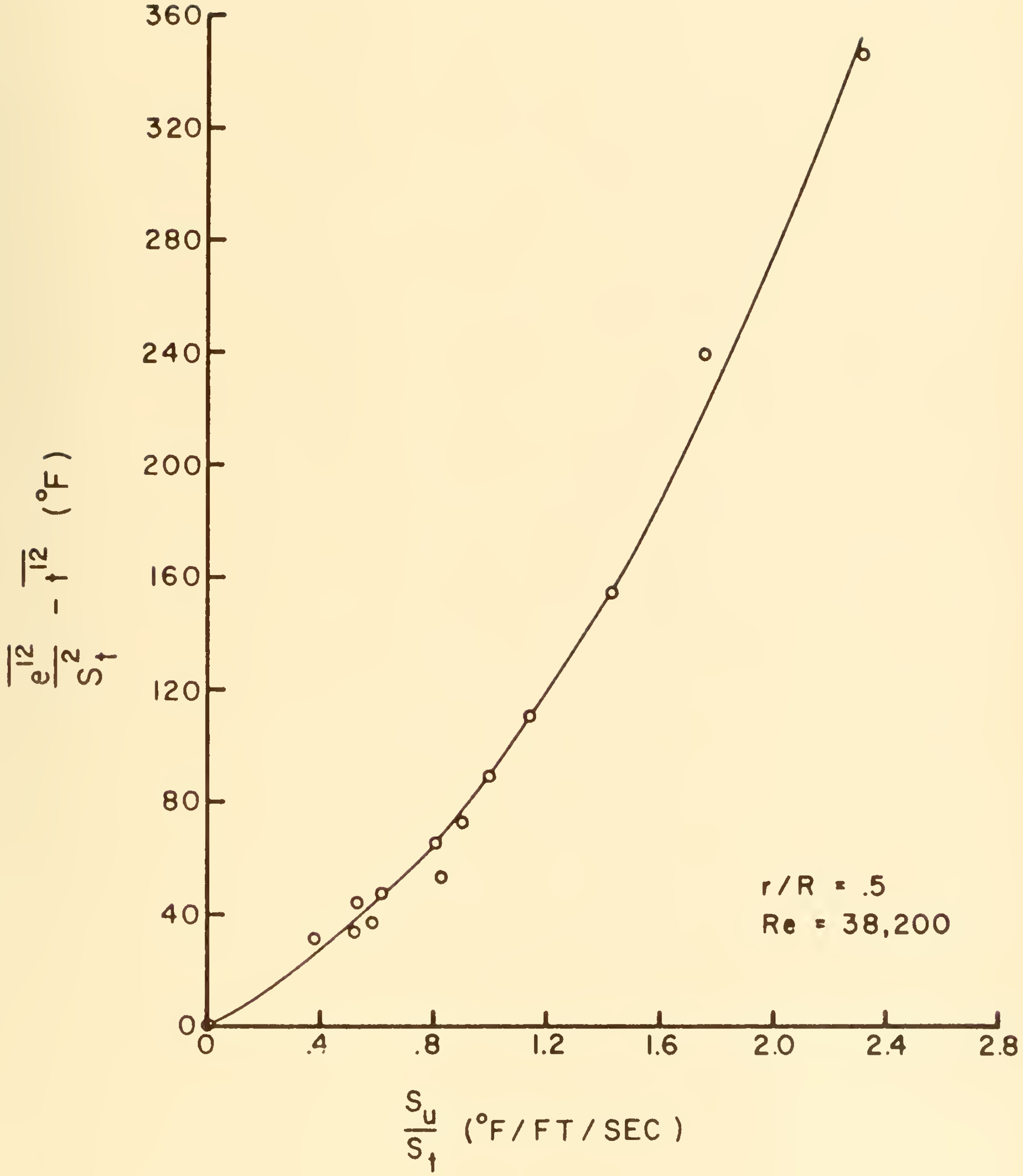

Figure 29. Kovasznay Fluctuation Diagram III

APPENDIX I

APPENDIX I

ERROR ANALYSIS

The results of the isothermal flow measurements with the hot-wire deviate from the results of Sandborn[11] and Laufer[10] by less than 10 percent.

The results of a preliminary non-isothermal run duplicating the conditions of Rodriguez-Ramirez and using the rapid response thermocouple agreed with his results within 5 percent.

Since the errors in the results of the non-isothermal flow measurements with the hot-wire are quite large, a detailed estimate of their magnitude is needed.

It is assumed that the errors in $\sqrt{\overline{u'^2}}/\bar{u}_{\mathfrak{L}}$ and $\overline{u't'}/\bar{u}_{\mathfrak{L}}\ (T_o-T_{\mathfrak{L}})$ are primarily the result of errors in S_u and S_T. In order to obtain an estimate of the errors in S_u and S_T, an analysis was made of the discrepancies between successive calibrations as tabulated in Table 18.

Note that the actual errors in S_u and S_T come from a continuous drift in $\bar{E}$ during a given calibration as outlined in the DISCUSSION section. Since it is not possible to measure this drift, recourse was made to analyzing by this method. Thus the error estimates obtained below do not represent.confidence limits on the results but only rough approximations to the confidence limits. In Table 18 , the largest

discrepancies occur for $\bar{u}$ = 137 ft/sec. The percentage error, based on the before value, between the before and after values, was determined for each entry in the 137 ft/sec column. All the S_T errors were summed and divided by the number of entries and likewise for S_u. Thus, average errors were determined to be 19 percent in S_u and 14 percent in S_T.

The propagation of these errors into the coordinates of the Kovasznay Fluctuation Diagram is as follows:

$$\frac{\Delta\left(\dfrac{\overline{e'^2} - \overline{t'^2}}{S_T^2}\right)}{\dfrac{\overline{e'^2} - \overline{t'^2}}{S_T^2}} = 2\,\frac{\Delta S_T}{S_T} = 28 \text{ percent.}$$

$$\frac{\Delta\left(\dfrac{S_u}{S_T}\right)}{\dfrac{S_u}{S_T}} = \frac{\Delta S_u}{S_u} + \frac{\Delta S_T}{S_T} = 33 \text{ percent.}$$

These errors were assumed to apply to all values of $\bar{u}$ and r/R.

The value of $\frac{S_u}{S_T}$ for each point of the Kovasznay Fluctuation Diagram for $\bar{u}$ = 66 ft/sec r/R = 0 was increased by 33 percent, and the value of $\frac{\overline{e'^2} - \overline{t'^2}}{S_T^2}$ was decreased by 28 percent. A parabola was fitted to the resulting points and $\overline{u'^2}$ and $\overline{u't'}$ determined. The new values differed from the original values by 72 percent and 100 percent respectively. Since

$$\Delta\,\frac{\sqrt{\overline{u'^2}}}{\overline{u'^2}} = \frac{1}{2}\,\Delta\,\frac{\overline{u'^2}}{\overline{u'^2}}$$

the error in $\sqrt{\overline{u'^2}}$ is 36 percent. This 36 percent error was used as the limit of error for all values of $\sqrt{\overline{u'^2}}/u_{\text{℄}}$, and 100 percent was used for all values of $\overline{u't'}/\bar{u}_{cL}(T_o-T_{\text{℄}})$.